BMI 8-5101-JR-28 Dec 62

N 64 13402 #

NASA CR 55263

RESEARCH REPORT

BATTELLE
MEMORIAL INSTITUTE

BATTELLE FIELDS OF RESEARCH

AERONAUTICAL ENGINEERING
AGRICULTURAL CHEMICALS
ALLOY DEVELOPMENT
ANALYTICAL CHEMISTRY
APPLIED MATHEMATICS
BIOCHEMISTRY
BIOPHYSICS
BUILDING AND ENGINEERING MATERIALS
CATALYSIS AND SURFACE CHEMISTRY
CERAMICS
CHEMICAL ENGINEERING
CHEMICAL PROCESSES
CORROSION TECHNOLOGY
COMPUTER ENGINEERING
ECONOMICS
ELECTRICAL ENGINEERING
ELECTROCHEMICAL ENGINEERING
ELECTROCHEMISTRY
EXTRACTIVE METALLURGY
ELECTRONICS
FERROUS METALLURGY
FOUNDRY PRACTICE
FOOD TECHNOLOGY
FUELS AND COMBUSTION
GRAPHIC ARTS TECHNOLOGY
GLASS TECHNOLOGY
HIGH-TEMPERATURE METALLURGY
HUMAN ENGINEERING
IMMUNOLOGY AND CANCER STUDIES
INDUSTRIAL PHYSICS
INFORMATION PROCESSING
INORGANIC CHEMISTRY

INSTRUMENTATION
LIGHT ALLOYS AND RARE METALS
LUBRICANT TECHNOLOGY
MECHANICAL ENGINEERING
METAL FINISHING
METALLURGICAL PROCESSES
MINERALOGY AND MICROSCOPY
MINERALS PROCESSING
MICROBIOLOGY
NONFERROUS METALLURGY
NUCLEONICS
OPERATIONS RESEARCH
ORGANIC CHEMISTRY
ORGANIC COATINGS
PETROCHEMICALS
PETROLEUM ENGINEERING
PHYSICAL CHEMISTRY
PHARMACEUTICAL CHEMISTRY
PRODUCTION ENGINEERING
PULP AND PAPER TECHNOLOGY
RADIOISOTOPES AND RADIATION
RELIABILITY ENGINEERING
REACTOR TECHNOLOGY
REFRACTORIES
RUBBER AND PLASTICS
SEMICONDUCTORS AND SOLID-STATE DEVICES
SYSTEMS ENGINEERING
TEXTILES AND FIBERS
THEORETICAL AND APPLIED MECHANICS
THERMODYNAMICS
WELDING AND METALS-JOINING TECHNOLOGY
WOOD AND FOREST PRODUCTS

SUMMARY REPORT

on

SPACE-VEHICLE STABILIZED-PLATFORM
GIMBAL-SYSTEM WEIGHT-REDUCTION STUDY.

PHASE I.   DESIGN OF RING GIMBALS

NAS 8-5101)

to

GEORGE C. MARSHALL
SPACE FLIGHT CENTER

December 28, 1962

by

J. E. Sorenson, J. C. Gerdeen, L. E. Hulbert,
T. J. Atterbury, and G. M. McClure

BATTELLE MEMORIAL INSTITUTE
505 King Avenue
Columbus 1, Ohio

BATTELLE FIELDS OF RESEARCH

AERONAUTICAL ENGINEERING
AGRICULTURAL CHEMICALS
ALLOY DEVELOPMENT
ANALYTICAL CHEMISTRY
APPLIED MATHEMATICS
BIOCHEMISTRY
BIOPHYSICS
BUILDING AND ENGINEERING MATERIALS
CATALYSIS AND SURFACE CHEMISTRY
CERAMICS
CHEMICAL ENGINEERING
CHEMICAL PROCESSES
CORROSION TECHNOLOGY
COMPUTER ENGINEERING
ECONOMICS
ELECTRICAL ENGINEERING
ELECTROCHEMICAL ENGINEERING
ELECTROCHEMISTRY
EXTRACTIVE METALLURGY
ELECTRONICS
FERROUS METALLURGY
FOUNDRY PRACTICE
FOOD TECHNOLOGY
FUELS AND COMBUSTION

INSTRUMENTATION
LIGHT ALLOYS AND RARE METALS
LUBRICANT TECHNOLOGY
MECHANICAL ENGINEERING
METAL FINISHING
METALLURGICAL PROCESSES
MINERALOGY AND MICROSCOPY
MINERALS PROCESSING
MICROBIOLOGY
NONFERROUS METALLURGY
NUCLEONICS
OPERATIONS RESEARCH
ORGANIC CHEMISTRY
ORGANIC COATINGS
PETROCHEMICALS
PETROLEUM ENGINEERING
PHYSICAL CHEMISTRY
PHARMACEUTICAL CHEMISTRY
PRODUCTION ENGINEERING
PULP AND PAPER TECHNOLOGY
RADIOISOTOPES AND RADIATION
RELIABILITY ENGINEERING
REACTOR TECHNOLOGY
REFRACTORIES

ABSTRACT

13 402

This report describes the analysis and design synthesis of the supporting structure of a stabilized platform, the primary objective being to minimize the weight of the supporting gimbals. The analysis resulted in an over-all weight reduction of 24.53 pounds (calculated) in the supporting structure (original weight — 54.41 pounds) with only a 16 per cent reduction (calculated) in the lowest system response frequency.

Considered in the analysis were stresses and deflections for an 8-g linear acceleration. The calculations were carried out with the aid of a Bendix G-20 digital computer. A generalized stiffness-matrix computer program was written for this problem and was used to calculate the displacements for various loading conditions. The stresses were calculated by means of an additional program used in conjunction with the stiffness-matrix program. The redesigned structure was then analyzed for response frequencies.

This research program was initiated in July, 1962, under contract with NASA and covers work performed during the period July 1, 1962, to December 28, 1962. *Author*

TABLE OF CONTENTS

SPACE-VEHICLE STABILIZED-PLATFORM GIMBAL-SYSTEM WEIGHT-REDUCTION STUDY

PHASE I. DESIGN OF RING GIMBALS

by

J. E. Sorenson, J. C. Gerdeen, L. E. Hulbert,
T. J. Atterbury, and G. M. McClure

INTRODUCTION

The importance of reducing the dead weight in the final stages of ballistic missiles and space vehicles becomes apparent when one examines the launching weight-to-payload ratios. For a two-stage ballistic missile, this ratio is approximately 42.[1]* This implies that a 1-pound reduction in the payload results in a 42-pound reduction in the launching weight of this type of vehicle. When the payload must be accelerated to orbital velocity, this ratio is much higher. It has been stated[1] that each additional pound of satellite results in an addition of 10,000 pounds to the launching weight of the vehicle. Therefore, it appears that any reduction in the payload dead weight results in a substantial reduction in the final vehicle weight.

With this emphasis placed on achieving minimum weight, critical examinations are made of the design of each component. In the Saturn vehicle, the supporting gimbals of the stabilized platform appear to have more weight than is necessary to perform their function.

The ST-124 inertial platform weighs approximately 110 pounds (excluding the hemispherical covers). The supporting structure (gimbals and frame) accounts for approximately 49.5 per cent or 54.4 pounds (excluding the trunnions). This research program was undertaken to reduce the weight of these supporting members as much as possible without exceeding predetermined stress or stiffness limits at any point in the assembly — at the same time, keeping the over-all dimensions of the inertial platform the same, and retaining all of the present components (support trunnions, gyros, electronic components, etc.)

After an examination of the problem, it was decided to channel the research effort into three parallel studies:

- A materials investigation

- An engineering study

- A design synthesis using stress, deflection, and vibration programs written for Battelle's Bendix G-20 digital computer.

Various materials were studied to determine the best one for a minimum weight design. The problem was not simply to select the material with the best strength-to-weight ratio, but to examine all of the mechanical properties and methods of fabrication and determine their relative importance in this design.

---

* References are listed at the end of this report.

The engineering study consisted of examining all the components of the ST-124 inertial platform and their relation to the size of the supporting gimbals. Also, a stress analysis of the gimbals was undertaken, using available theoretical load-stress relations. This was necessary to insure that the computer study resulted in a practical design. The frame with its covers was considered a spherical shell. Design was based upon theory of shells.

The design synthesis began by writing the necessary computer programs to calculate stress, deflection, and natural frequency for various loading conditions. After completion of these programs, results from the engineering study were used for the first typical design. The stresses and deflections in this design were then calculated for various loading conditions with the aid of these programs. After examination of these data (stresses, deflections, and response frequencies), modifications were made in the design at points of high and low stress and a new set of input data was formulated. The stresses and deflections were then calculated for this revised design. This iteration process continued until the critical design factors reached their limiting values.

RESULTS AND RECOMMENDATIONS

As a result of the analysis, the recommended configuration of the structural components is shown on Drawings 1001, 1002, 1003, and 1004 attached to this report.

The material recommended for the gimbals is beryllium. As will be discussed later in this report, stiffness rather than strength is the controlling factor in the design. Beryllium with its high stiffness-to-weight ratio is the best available material for a minimum weight design.

The over-all weight reduction achieved is 24.53 pounds. This represents a 50.5 per cent reduction in the weight of the structural components analyzed. In order to minimize the weight of the supporting frame, the hemispherical covers were considered as part of the load-carrying structure. That is, the frame was considered as a spherical shell in the calculations. Aluminum is recommended for the frame because it is relatively easy to fabricate into any shape. Alloys from the 5000 series are preferred for the wrought components because of their formability, weldability, and strength. For sand or permanent-mold cast parts with thin sections, a high-silicon grade, such as 356 is suggested.

Table 1 gives a comparison of the weights of these structural members.

TABLE 1. WEIGHTS OF THE PRIMARY STRUCTURAL MEMBERS

| | Weight, pounds | | |
Member	Present Design	Proposed Design	Net Reduction
Inner gimbal casting (Be)	5.87	5.87	--
Middle gimbal casting (Be)	7.93	3.02	4.91
Outer gimbal casting (Be)	5.96	2.65	3.31
Redundant gimbal casting (Be)	12.30	5.44	6.86
Frame (Al)	22.35	12.90	9.45
TOTALS	54.41	29.88	24.53

The following sections discuss the important factors considered in the design.

Stresses and Deflections

The stresses resulting from an 8-g linear acceleration are shown for each gimbal in Appendix C (Figures C-2 to C-12). The deflections at various points in the assembly are shown in Tables C-1 to C-8 in Appendix C. Both stresses and deflections are shown for acceleration in each of the three directions X, Y, and Z. For a specific point in the assembly, the maximum possible primary stress, due to bending moments, occurs for a particular orientation of the acceleration vector. This stress is not shown but can be computed from the equations given in Appendix C. However, at no point does it exceed 5000 psi (neglecting any stress concentrations) in the proposed assembly. In the present assembly the maximum calculated bending stress is less than 2500 psi. With the use of

flanged sections, a secondary flange bending stress results with torsional loads. This stress occurs at the junction of the flanged section with the heavier trunnion area in the middle and outer gimbals. The value of this stress depends on the stiffness of the trunnions or the amount of external torsional restraint applied to the gimbal. This stress is a maximum when the acceleration is normal to the plane of the gimbal (X direction for the middle gimbal and Y direction for the outer gimbal). The possible range of this stress is 3000 psi (rigid trunnions) to 11,000 psi (flexible trunnions) for the middle gimbal, and 2000 psi to 10,000 psi for the outer gimbal. However, the trunnions are not completely flexible and therefore the value of this stress will be less than the maximum value shown.

These higher-stressed areas are marked on the drawings. Because of the notch sensitivity of beryllium, it is important to avoid creating any stress concentrations in the vicinity of these high stresses. Therefore, care should be exercised in the fabrication of these gimbals to avoid placing any notch, hole, or sharp change in section in these areas.

A comparison of the maximum displacement of the inner gimbal in the present and proposed designs is shown in Table 2. A large portion of this displacement occurs in the redundant gimbal and is due to the relatively low torsional stiffness of this member.

TABLE 2. DISPLACEMENT OF THE INNER GIMBAL FOR AN 8-G LINEAR ACCELERATION IN THE +Y DIRECTION

Relative Stiffness of Trunnions	Displacement, 10^{-6} inches	
	Present Design	Proposed Design
Flexible	3784	5325
Rigid	807	1254

The terms "flexible" and "rigid" are used to describe the relative stiffness of the trunnions. The stresses and deflections for each condition represent the upper and lower limits. For example, if the trunnions are very stiff, the stresses and deflections will then approach the values shown for rigid trunnions. At the other extreme, if the trunnions are relatively flexible, the stresses and deflections will approach the values given for flexible trunnions.

Response Frequencies

The response frequencies of the gimbals for various mode shapes are shown in Table 3. The lowest response frequencies of the systems are shown in Table 4.

If the system response frequency is lower than desirable, two possibilities exist for increasing it without inflicting a severe weight penalty on the system. First, a large portion of the deflection, when the acceleration is in the Y direction, is due to the low torsional stiffness of the redundant gimbal. When the loads are normal to the plane of

TABLE 3. LOWEST RESPONSE FREQUENCIES OF THE GIMBALS

| | Frequency, cps | | | | | |
| | X | | Y | | Z | |
Gimbal	Present Design	Proposed Design	Present Design	Proposed Design	Present Design	Proposed Design
Simply Supported at Two Points (180 Degrees Apart) With No Supported Mass						
Middle	1200	464	1375	1052	1195	1001
Outer	2060	1900	1685	968	2340	2140
Redundant	1055	672	390	368	925	673
Simply Supported at Two Points (180 Degrees Apart) With One-Half the Mass of the Inner Components Concentrated at Points 90 Degrees From the Supports						
Middle	581	231	643	520	622	514
Outer	760	626	560	302	715	640
Redundant	368	235	153	138	415	269

TABLE 4. LOWEST RESPONSE FREQUENCIES OF THE SYSTEM

| Relative Stiffness of the Trunnions | Frequency, cps | | | | | |
| | X | | Y | | Z | |
	Present Design	Proposed Design	Present Design	Proposed Design	Present Design	Proposed Design
Flexible	288	163	144	121	311	224
Rigid	358	246	309	254	388	285

the gimbal, the gimbal sections are subjected to torsional loads and, if allowed to twist, a large deflection will result at the points of loading. Therefore, the response frequency can be increased by increasing the stiffness of the trunnions, especially those of the redundant and outer gimbals. This would have the same effect as increasing the torsional stiffness of the redundant gimbal. Second, the redundant gimbal itself could be modified in such a manner as to increase its torsional stiffness.

The torsional stiffness of a beam with a rectangular cross section of width b, and thickness h, is[2]:

$$S = \frac{T}{\theta} = \frac{b\,h^3 G\,\beta}{L}$$

where

S = torsional stiffness

T = torque, in-lb

θ = angle of twist, radians

L = length of beam, inches

β = function of b/h

   b/h = 1, β = 0.141

   b/h = 10, β = 0.312

   b/h = ∞, β = 0.333

G = shearing modulus of elasticity, lb/in.^{2}.

This equation indicates that the thickness, h, of the redundant gimbal should be increased as much as possible in order to increase the torsional stiffness in the most economical fashion. Calculations indicate that if the redundant gimbal cross section approximates a rectangle, 2-1/2 x 5/8 inch, the lowest system response frequency could be increased by 40 per cent over that of the proposed design and 16 per cent over the present design. This magnitude of increased stiffness is not believed necessary for the proposed design. This is pointed out as a simple method to increase system frequency should it ever be required.

Frame Design

The frame was designed as a portion of a spherical shell. For such a shell, made of aluminum and having a spherical diameter of 19.50 inches and a thickness of 0.050-inch, the maximum deflection, rotation, and stress would be:

   Maximum deflection (w) = 1260×10^{-6} inches

   Maximum stress (σ) = 4920 psi

   Maximum rotation ($\Delta\phi$) = 194×10^{-6} radians (40 seconds).

The maximum deflection and stress occur in the shell next to the Z pivot supports for an acceleration of 8 g at an angle of approximately 60 degrees to the Z axis. The maximum rotation is for the Z pivot support for an 8 g acceleration in the X direction. A natural frequency, f_n, of at least 350 cps could be expected. Conservative calculations were conducted to determine w, σ, $\Delta\phi$, and f_n. Actual w, σ, and $\Delta\phi$ would be expected to be lower than above, and actual f_n would be expected to be higher.

MATERIALS INVESTIGATION

Data on high-strength alloys which may have applications in this design were assembled. Particular emphasis was placed on beryllium[3], since it appears very attractive because of its high strength-to-weight and elastic modulus-to-weight ratios. The preliminary study resulted in five candidate materials. The materials and their properties are shown in Table 5. Flexibility in fabrication techniques was also considered in this investigation.

A comparison of the five materials was first made using the material-index approach. This comparison, using the strength-to-weight and modulus-to-weight ratios as the indexes, is shown in Table 6.

The effect of the section geometry on the relative weights of rings fabricated from the different materials is shown in Table 7. The comparison was made first for rings with the same load-deflection (in-plane loading) characteristics and second for rings with the same load-yield strength characteristics. The properties given in Table 5 were used in these comparisons.

Another factor that must be considered in this design is the natural frequency of the gimbals. Since the natural frequency is a function of the mass and deflection, the relative weights shown for rings with the same load-deflection characteristic are also the relative weights of rings with the same natural frequency (in-plane mode shapes).

On the basis of these comparisons, it appears that beryllium is the best material (for minimum weight) when deflection or vibration is the criterion. However, when the strength is the criterion, titanium appears to be the best available material for a minimum-weight design. It is shown later in the study that vibration and stiffness are the most important design criteria.

Machining the rings from hot-pressed blocks is expected to be the most satisfactory method of fabrication within present technology. Higher strength forms of beryllium now becoming available do not offer particular advantages because the strength is not fully utilized. Because of beryllium notch sensitivity, insofar as possible, holes, discontinuities, etc., should not be located in the higher stressed areas marked on the drawings.

TABLE 5. MECHANICAL AND PHYSICAL PROPERTIES OF CANDIDATE MATERIALS

	Unit	Beryllium QMV, Vacuum Hot Pressed	Aluminum 7075-T6, Die Forging	Magnesium AZ80A-T5, Forging	Steel 4340 HT260, Forging	Titanium B-120VCA, STA, Forging
Ultimate Tensile Strength (Min)	10^3 psi	33	71-75	42	260	190
Tensile Yield Strength, 0.2% (Min)	10^3 psi	27	62-65	28	217	170
Ultimate Shear Strength (Min)	10^3 psi	39(a)	45	20	149	
Shear Yield Strength, 0.2% (Min)	10^3 psi	18.6				
Precision Elastic Limit	10^3 psi	2-6				
E, Modulus of Elasticity	10^6 psi	43	10.3	6.5	29	16
G (Torsion) Shearing Modulus	10^6 psi	20	3.9	2.4	11	
Poission's Ratio (μ)		0.024 to 0.030	0.33			
Density (ρ)	lb/in.^{3}	0.067	0.101	0.0649	0.283	0.174
Specific Heat (C)	Btu/(lb)(F)	0.45 (at RT)	0.23 (at 212 F)	0.25 (at RT)	0.114 (at RT)	0.128 (at 100 F)
Thermal Conductivity (K)	Btu/[(hr)(ft^2)(F)/ft]	110 (at RT)	70 (at RT)	44 (212 to 572 F)	22 (at RT)	4 (at 100 F)
Coefficient of Linear Expansion (α)	10^{-6} in./in./F	11.6 (RT to 212 F)	13.1 (RT to 212 F)	14 (65 to 212 F)	6.3 (0 to 200 F)	4.8 (to 100 F)
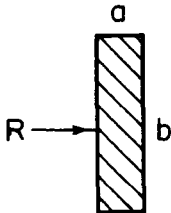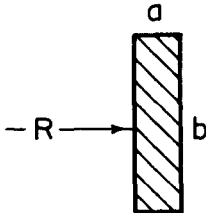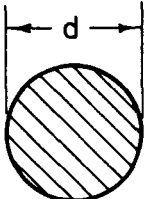
(a) Nominal or typical value in torsion.

TABLE 6. COMPARISON OF MATERIALS USING PHYSICAL AND
MECHANICAL PROPERTIES

Materials	Yield Strength-to-Weight Ratio $\left(\dfrac{\sigma_{ys}}{\rho}\right)$, $\dfrac{10^6 \text{ psi}}{\text{lb in.}^{-3}}$	Stiffness-to-Weight Ratio $\left(\dfrac{E}{\rho}\right)$, $\dfrac{10^6 \text{ psi}}{\text{lb in.}^{-3}}$
Beryllium (QMV)	404	642
Magnesium (AZ80A-T5)	430	100
Aluminum (7075-T6)	614	102
Steel (4340 HT260)	766	102
Titanium (B-120VCA)	976	92

TABLE 7. RELATIVE WEIGHTS OF RINGS OF DIFFERENT MATERIALS

	Relative Weight		
Material	I changed by varying a	I changed by varying b	I changed by varying d
Same Load[a]-Deflection Characteristics			
Beryllium (QMV)	1.00	1.00	1.00
Magnesium (AZ80A-T5)	1.82	6.42	2.50
Aluminum (7075-T6)	2.43	6.31	3.09
Steel (4340 HT260)	4.82	6.26	5.85
Titanium (B-120VCA)	3.60	7.00	4.26
Same Load[a]-Yield Strength Characteristics			
Beryllium (QMV)	1.00	1.00	1.00
Magnesium (AZ80A-T5)	0.95	0.94	0.95
Aluminum (7075-T6)	0.99	0.66	0.87
Steel (4340 HT260)	1.49	0.52	1.05
Titanium (B-120VCA)	1.04	0.41	0.76

(a) External load only (weight of ring assumed small in comparison to external load).

ENGINEERING STUDY

General

The present assembly was studied with the intention of minimizing any modifications in the gimbal components that might result from reductions in the size of the gimbal section. It is possible that, by reducing the section size, some components may have to be relocated or the method of mounting modified. By placing certain physical restrictions on the section geometry before completing the stress analysis, these modifications may be minimized.

These restrictions result from the following:

(1) The over-all size of the present assembly must be maintained. The size of each gimbal is restricted in the radial direction because of clearances between gimbals.

(2) The support trunnions used in the present assembly will be used in the new design. Therefore, there must be a sufficient amount of ring material at these points in order to mount the trunnions.

(3) Various components are mounted to the gimbal between the support points. The size of the gimbal must be such as to accommodate these components. Also, the minimum thickness of any section is limited because of the presence of threaded holes.

The section geometry also depends on the types of loads to which it is subjected. A minimum-weight design for a member subjected to bending only would consist of a section with a high section modulus-to-area ratio. This suggests the use of tubular or flanged sections (I, channel, etc.). However, when flanged sections are subjected to torsion, the torsional shearing stress and secondary flange bending stress (due to torsion) can become important.

Stress Analysis of Middle, Outer and Redundant Gimbals

Because of the complexity of the geometrical requirements for the inner gimbal, it appears that the weight reduction that could be achieved here is a rather small per cent of the total weight (probably less that 1 per cent without redesign and relocation of the inner gimbal components). It was therefore decided to maintain the present design of this gimbal and concentrate the research effort on the three other gimbals and the supporting frame.

The middle, outer, and redundant gimbals are approximate ring structures. The equations which apply to rings will therefore yield approximate solutions for these gimbals.

The first step in the analysis was to define the loads acting on each gimbal. The most general type of loading, resulting from inertial forces, is shown in Figure 1. In

13

A = Area of section

S_r = Section modulus about r axis
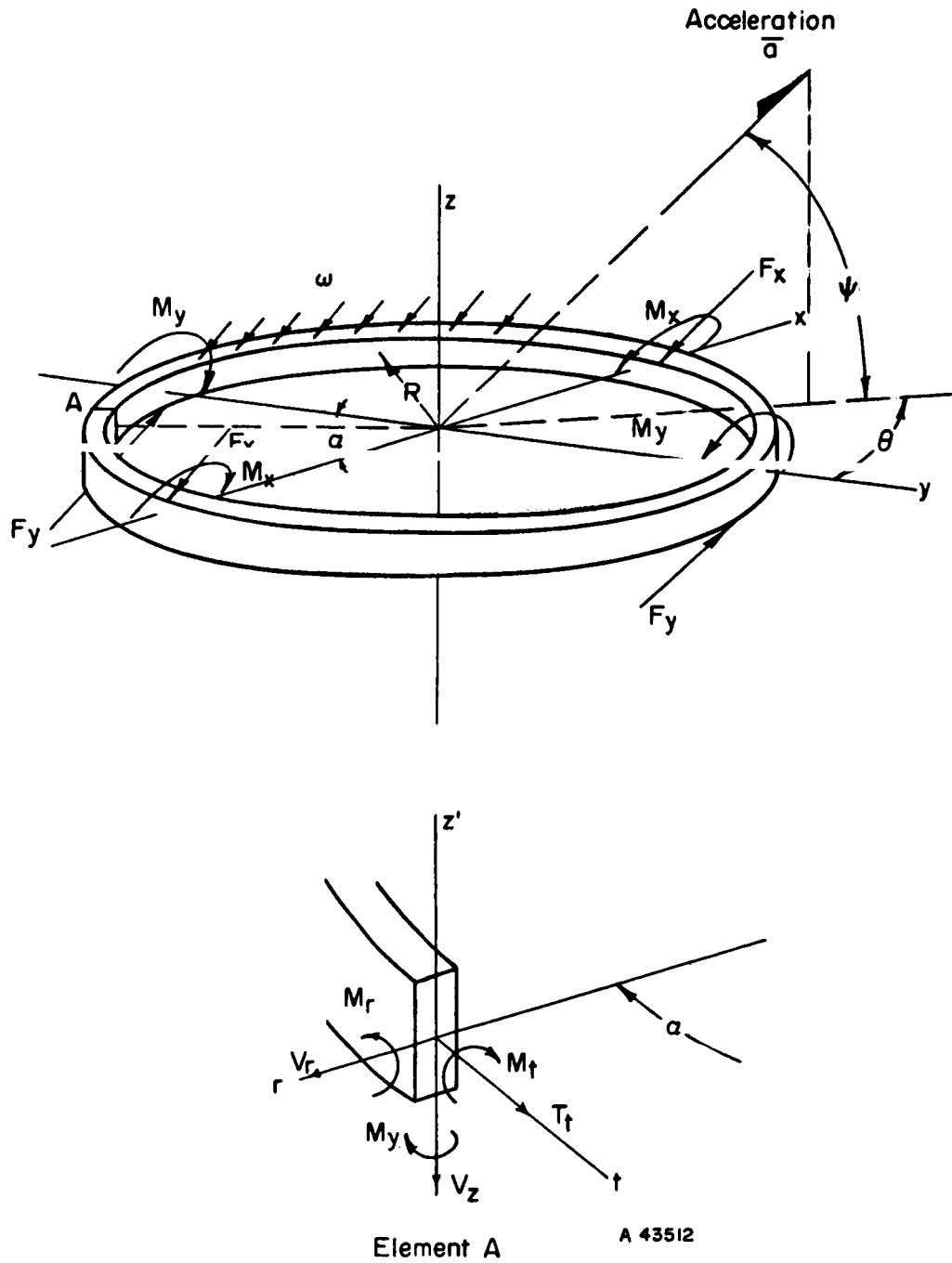
S_z = Section modulus about z axis

FIGURE 1. GENERALIZED LOADING CONDITIONS FOR A RING SUBJECTED TO INERTIAL FORCES

order to simplify the analysis, the forces were resolved into components acting in the direction of the frame reference axis (Figure 2). Each of the three cases shown in Figure 2 may be further resolved into simpler subcases involving only one type of load. Figure 3 shows the resulting seven subcases. The equations for the internal forces from each one of these subcases are given in Reference (4).

The nomenclature used in the following analysis is either given in Figure 1 or is included where necessary.

At a specific point in the ring, the equations for the internal forces are of the form (after algebraic summation from the appropriate subcases):

$$M_z = [(C_1 F_x R + C_2 \omega R^2 + C_3 M_y) \sin \theta$$
$$+ (C_4 F_x R + C_5 \omega R^2 + C_6 M_x) \cos \theta] \cos \Psi \tag{1}$$

$$T_t = [(C_7 F_x + C_8 \omega R + C_9 \frac{M_y}{R}) \sin \theta$$
$$+ (C_{10} F_x + C_{11} \omega R + C_{12} \frac{M_x}{R}) \cos \theta] \cos \Psi \tag{2}$$

$$V_r = [(C_{13} F_x + C_{14} \omega R + C_{15} \frac{M_y}{R}) \sin \theta$$
$$+ (C_{16} F_x + C_{17} \omega R + C_{18} \frac{M_x}{R}) \cos \theta] \cos \Psi \tag{3}$$

$$M_r = [C_{19} F_x R + C_{20} \omega R^2 + C_{21} M_y + C_{22} Mx] \sin \Psi \tag{4}$$

$$M_t = [C_{23} F_x R + C_{24} \omega R^2 + C_{25} M_y + C_{26} M_x] \sin \Psi \tag{5}$$

$$V_z = [C_{27} F_x + C_{28} \omega R] \sin \Psi, \tag{6}$$

where C_n are constants pertaining to a particular point in the ring. Substituting the values for F_x, R, ω, M_y, and M_x, the equations may be written:

$$M_z = [K_1 \sin \theta + K_2 \cos \theta] \cos \Psi$$

$$T_t = [K_3 \sin \theta + K_4 \cos \theta] \cos \Psi$$

$$V_r = [K_5 \sin \theta + K_6 \cos \theta] \cos \Psi$$

$$M_r = K_7 \sin \Psi$$

$$M_t = K_8 \sin \Psi$$

$$V_z = K_9 \sin \Psi,$$

where K_n are now constants for a specific point in the ring.
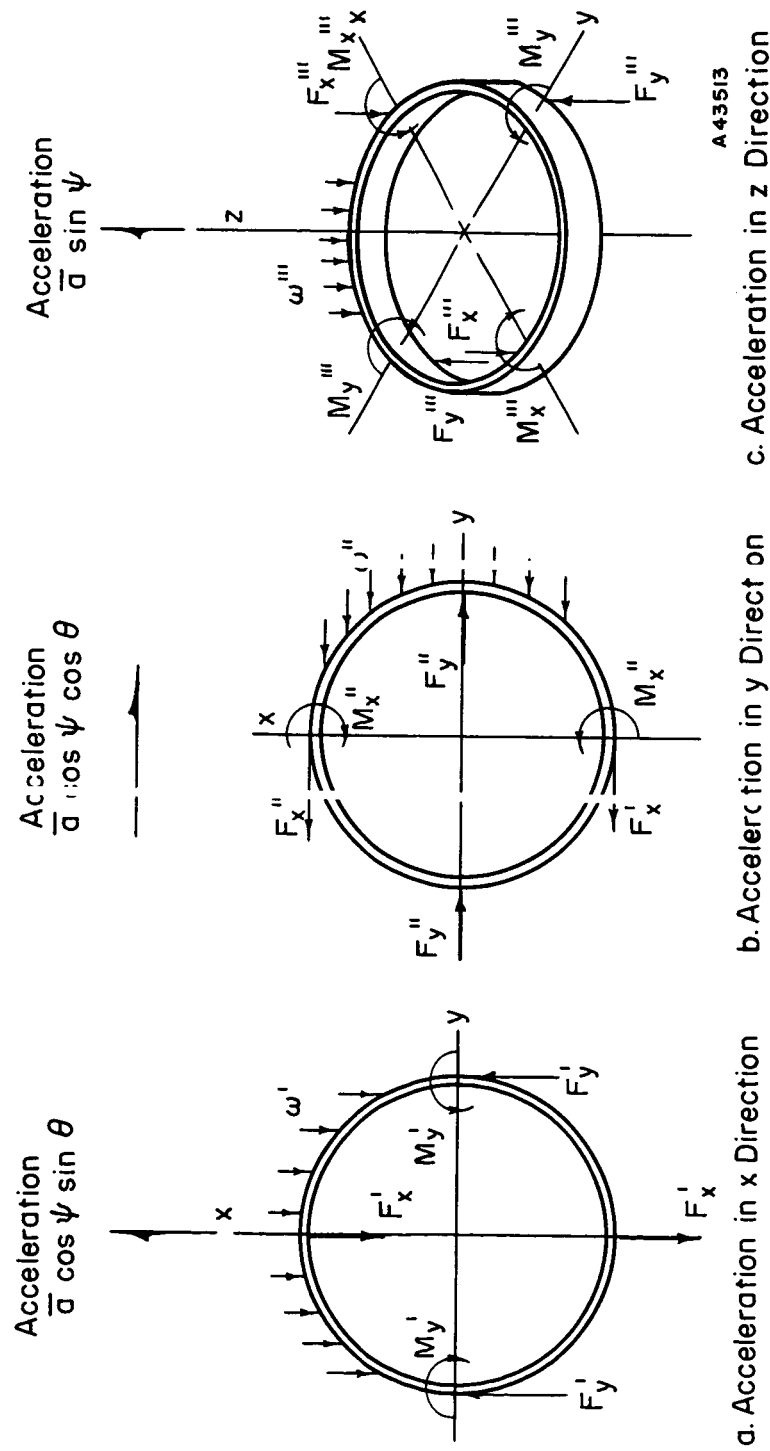
FIGURE 2. INERTIAL FORCES RESOLVED INTO THE THREE REFERENCE AXES

a. Acceleration in x Direction

b. Acceleration in y Direction

c. Acceleration in z Direction

Acceleration $\bar{a}\cos\psi\sin\theta$

Acceleration $\bar{a}\cos\psi\cos\theta$

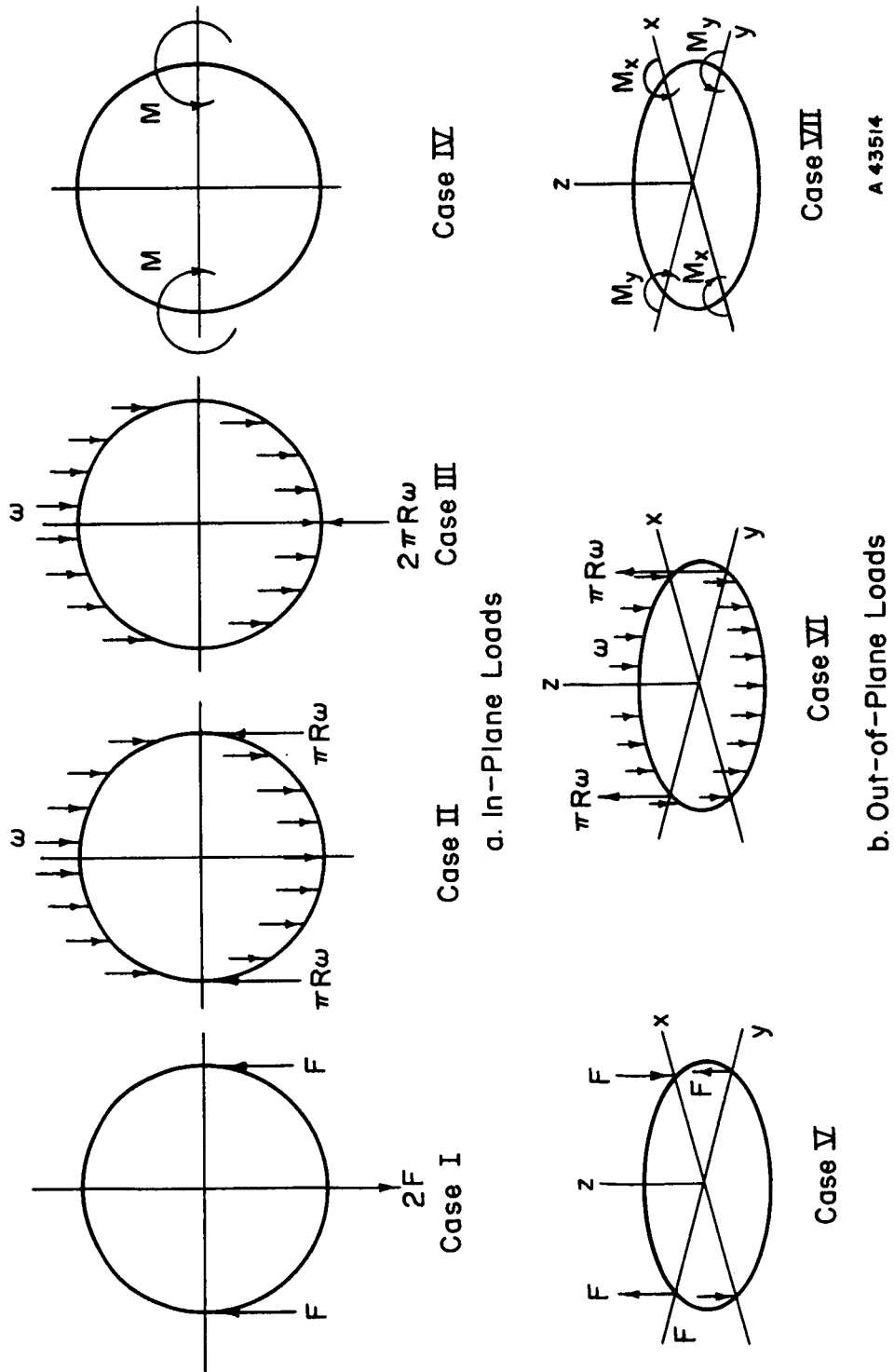Acceleration $\bar{a}\sin\psi$

A43513

FIGURE 3. GENERALIZED LOADING CONDITION RESOLVED INTO SIMPLE CASES

For rectangular, channel, or I sections, the normal stress at the outer corners (most extreme fiber) is:

$$\sigma = \frac{M_z}{S_z} + \frac{T_t}{A} + \frac{M_r}{S_r}$$

or

$$\sigma = \frac{[K_1 \sin \Theta + K_2 \cos \Theta]}{S_z} \cos \Psi + \frac{[K_3 \sin \Theta + K_4 \cos \Theta]}{A} \cos \Psi$$

$$+ \frac{K_7}{S_r} \sin \Psi. \tag{7}$$

This stress is a maximum when $\Theta = \Theta_m$, and $\Psi = \Psi_m$,

such that

$$\left. \frac{\partial \sigma}{\partial \Theta} \right]_{\Theta_m, \Psi_m} = 0 \tag{8}$$

and

$$\left. \frac{\partial \sigma}{\partial \Psi} \right|_{\Theta_m, \Psi_m} = 0 . \tag{9}$$

In order to simplify the calculations for Θ_m, it is assumed that the stress due to T_t is zero. This is valid if $\frac{T_t}{A} \ll \frac{M_z}{S_z}$.

$$\frac{\partial \sigma}{\partial \Theta} = [K_1 \cos \Theta - K_2 \sin \Theta] \frac{\cos \Psi}{S_z}$$

$$\left. \frac{\partial \sigma}{\partial \Theta} \right]_{\Theta_m, \Psi_m} = [K_1 \cos \Theta_m - K_2 \sin \Theta_m] \frac{\cos \Psi_m}{S_z} = 0 .$$

The equation is satisfied when $\Psi_m = \frac{\pi}{2}$ or

$$\Theta_m = \tan^{-1}\left[\frac{K_1}{K_2} \right]. \tag{10}$$

When $\Psi_m = \pi/2$, the acceleration is in the z direction, and the forces T_t and M_z are zero. Therefore, the general solution is given by Equation (10).

Satisfying the second condition (Equation 9),

$$\frac{\partial \sigma}{\partial \Psi} = - [K_1 \sin \Theta + K_2 \cos \Theta] \frac{\sin \Psi}{S_z}$$

$$- [K_3 \sin \Theta + K_4 \cos \Theta] \frac{\sin \Psi}{A} + \frac{K_7}{S_r} \cos \Psi$$

$$\left.\frac{\partial \sigma}{\partial \Psi}\right]_{\Theta_m, \Psi_m} = -\left[\left(\frac{K_1}{S_z} + \frac{K_3}{A}\right)\sin \Theta_m + \left(\frac{K_2}{S_z} + \frac{K_4}{A}\right)\cos \Theta_m\right]\sin \Psi_m$$

$$+ \frac{K_7}{S_r}\cos \Psi_m = 0.$$

This condition is satisfied when

$$\Psi_m = \tan^{-1}\left[\frac{K_7/S_r}{\left(\frac{K_1}{S_z} + \frac{K_3}{A}\right)\sin \Theta_m + \left(\frac{K_2}{S_z} + \frac{K_4}{A}\right)\cos \Theta_m}\right]. \tag{11}$$

Equation (7) may also be written,

$$\sigma = [\sigma_{Bx} \sin \Theta + \sigma_{By} \cos \Theta] \cos \Psi$$

$$+ [\sigma_{Tx} \sin \Theta + \sigma_{Ty} \cos \Theta] \cos \Psi + \sigma_{Bz} \sin \Psi,$$

where

σ_{Bx} = bending stress at point under consideration for acceleration in x direction.

σ_{By} = bending stress at point under consideration for acceleration in y direction.

σ_{Bz} = bending stress at point under consideration for acceleration in z direction.

σ_{Tx} = tensile stress at point under consideration for acceleration in x direction.

σ_{Ty} = tensile stress at point under consideration for acceleration in y direction.

The equations for Θ_m and Ψ_m become

$$\Theta_m = \tan^{-1}\left[\frac{\sigma_{Bx}}{\sigma_{By}}\right] \tag{12}$$

and

$$\Psi_m = \tan^{-1}\left[\frac{\sigma_{Bz}}{\sigma_{Bxy} + \sigma_{Txy}}\right]. \tag{13}$$

The maximum stress, σ_{max}, at a specific section in the ring occurs when the orientation of the acceleration vector is Θ_m and Ψ_m, and is

$$\sigma_{max} = [\sigma_{Bx} \sin \Theta_m + \sigma_{By} \cos \Theta_m] \cos \Psi_m$$

$$+ [\sigma_{Tx} \sin \Theta_m + \sigma_{Ty} \cos \Theta_m] \cos \Psi_m + \sigma_{Bz} \sin \Psi_m. \tag{14}$$

At any other orientation of the acceleration vector, the fiber stress at this section is less than that given by Equation (14).

The shearing stress was computed in a similar manner.

This is the method used to make the first approximation for the various cross sections. Neglected in the calculations was the secondary flange bending (for channels and I sections) due to M_t. This will be accounted for in the analytical study using the computer. Also in this design, limits were placed on the size of the sections because of the physical restrictions. Vibration was also neglected in this approach but is included in the computer analysis.

The values for C_n are given in Appendix A for 15-degree increments around the ring.

Stress Analysis of Frame

Weight reduction on the frame was considered by changing its configuration from that of a ring to that of a segment of a spherical shell in order to take advantage of increased rigidity from double curvature. To aid the analysis, the frame and the adjoining spherical covers were considered together to constitute a complete spherical shell with two trunion openings and additional reinforcements for assembly and mounting purposes. For ease of fabrication of the shell, aluminum was considered as the material. Here again beryllium would be the best choice of material from the property-index standpoint, but it is not within present technology to fabricate the shell structure of this material. The material constants for the analysis were:

$$\text{Modulus of Elasticity (E)} = 10 \times 10^6 \text{ psi}$$

$$\text{Poisson's ratio } (\mu) = 0.33 \tag{15}$$

$$\text{Density } (\rho) = 0.101 \text{ lb/in.}^3$$

(The analysis would also apply if the frame portion of the shell were made of ALMAG 35 which has material constants nearly the same as those of aluminum.) The shell dimensions used for calculation were:

$$\text{Spherical shell radius (a)} = 9.75 \text{ in.}$$

$$\text{Outer trunion radius (b)} = 3.12 \text{ in.} \tag{16}$$

$$\text{Shell thickness (t)} = 0.050 \text{ in.}$$

(The thickness t = 0.050 inch was found to give sufficiently low stress and deflections, and high natural frequency. Calculations are illustrated for this thickness.)

To obtain an indication of stress level, representative membrane stresses were first calculated. Method of calculation was similar to that described by Flügge, Reference (5), pages 60-66. Figures 4 and 5 show the membrane forces N_Θ, N_ϕ, and $N_{\Theta\phi}$ around the Θ = 0-degree and Θ = 90-degree meridians, respectively, from the shell's own inertia load p where:

FIGURE 4. MEMBRANE FORCES AROUND $\theta = \phi$ DEGREE MERIDIAN FROM INERTIA LOADING IN Y DIRECTION OF SPHERICAL SHELL (FRAME) WHEN SUPPORTED AT THREE POINTS ON EQUATOR

p = own inertia load, lb/in.^{2}

$$= \frac{\rho t A_Y}{g}$$

$N_\theta, N_\phi, N_{\theta\phi}$ = membrane forces, lb/in.

A43516
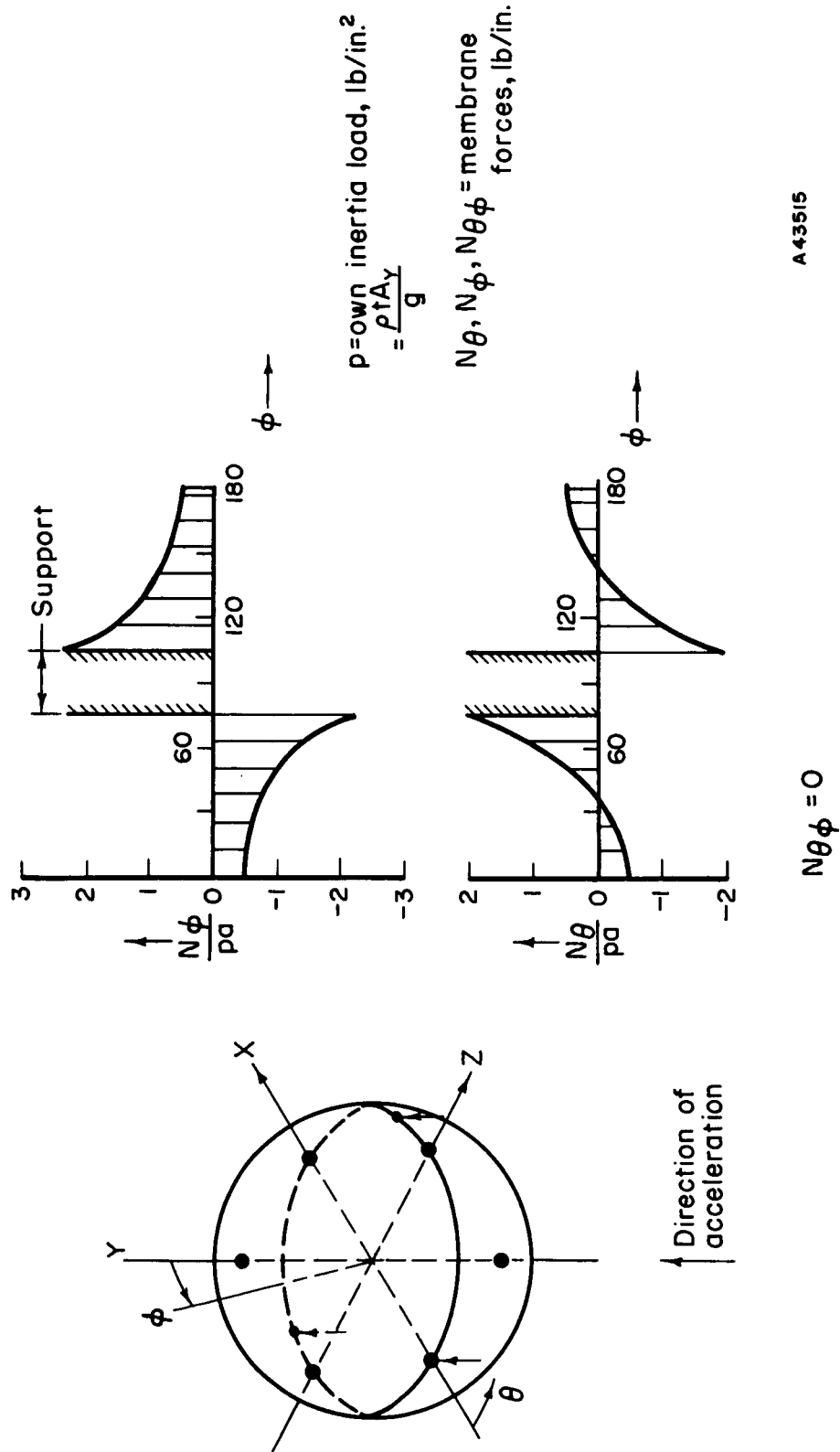

FIGURE 5. MEMBRANE FORCES AROUND $\theta = 90$-DEGREE MERIDIAN FROM INERTIA LOADING IN Y DIRECTION OF SPHERICAL SHELL (FRAME) WHEN SUPPORTED AT THREE POINTS ON EQUATOR
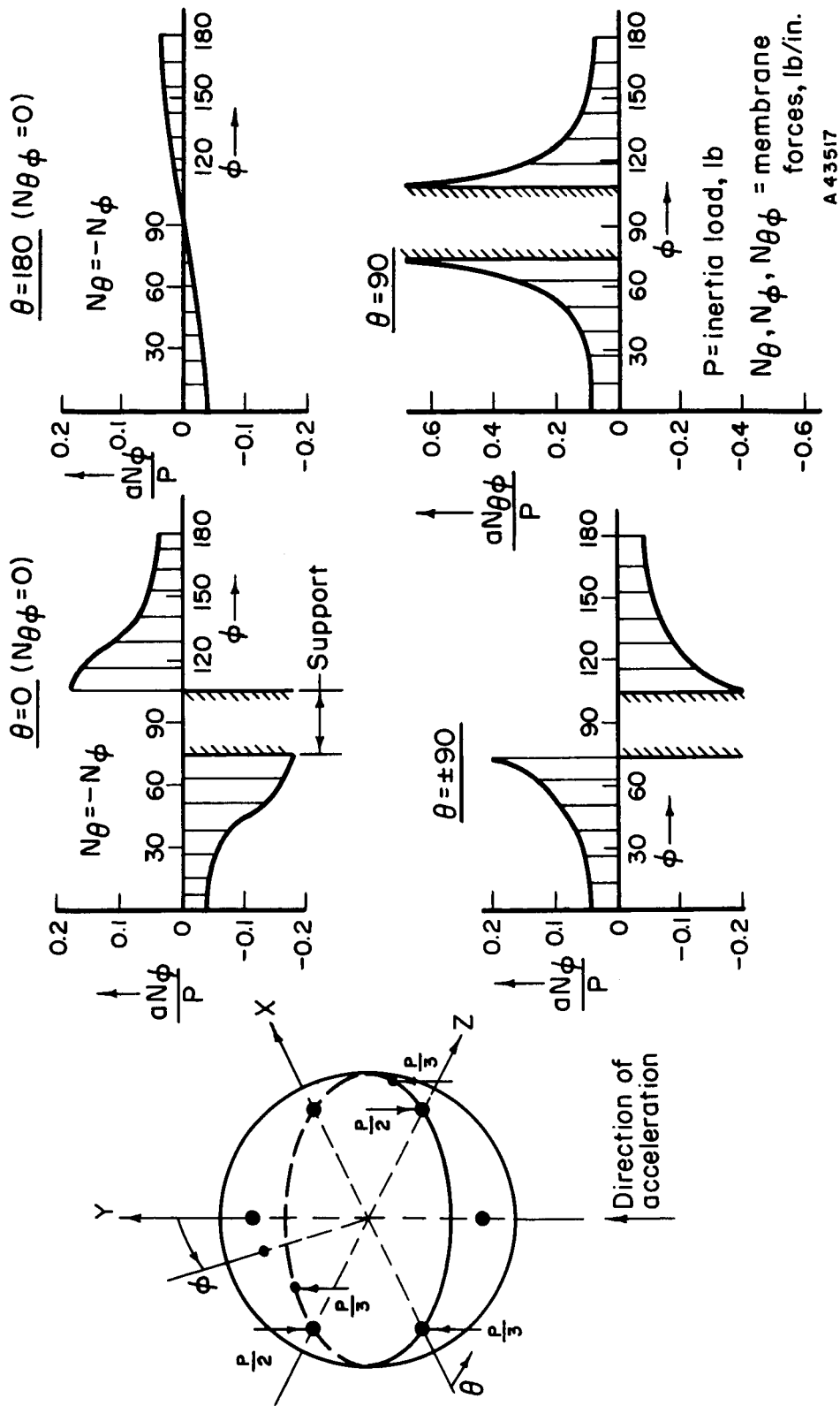
FIGURE 6. MEMBRANE FORCES FROM ATTACHED INERTIA LOADING IN Y DIRECTION OF SPHERICAL SHELL (FRAME) WHEN SUPPORTED AT THREE POINTS ON EQUATOR.

$$p = \frac{pt A_Y}{g} = lb/in.^2 \qquad (18)$$

A_Y = acceleration in Y
direction = 8 g .

The maximum membrane forces (maximum at the supports) in Figures 4 and 5 correspond to membrane stresses of only 20 psi.

Figure 6 shows the membrane forces from attached inertia loading, of total load P. For an inner mass of 65 pounds plus the weight of the +Z and -Z pivots, about 3 and 5 pounds respectively, the inertia load P for 8-g acceleration is:

$$P = 8 (65 + 3 + 5) = 8 (73) = 584 \, lb. \qquad (19)$$

The corresponding membrane stresses for this load are on the order of 1000 psi maximum.

The membrane theory gives only a partial indication of the stress level. General shell theory (membrane plus bending) must also be applied to determine the bending effects around the pivot supports through which the attached inertia loading is transmitted to the shell. Since the bending effects are localized (they are out rapidly with increasing distance from support), effects from opposite supports do not superimpose, and can be calculated by considering loading only on one support. The loadings considered are shown in Figure 7. Because of the large thickness of the pivot support (ring), it can be considered to be quite stiff compared to the shell.

FIGURE 7. TYPES OF LOADINGS AT PIVOT
SUPPORT ON FRAME

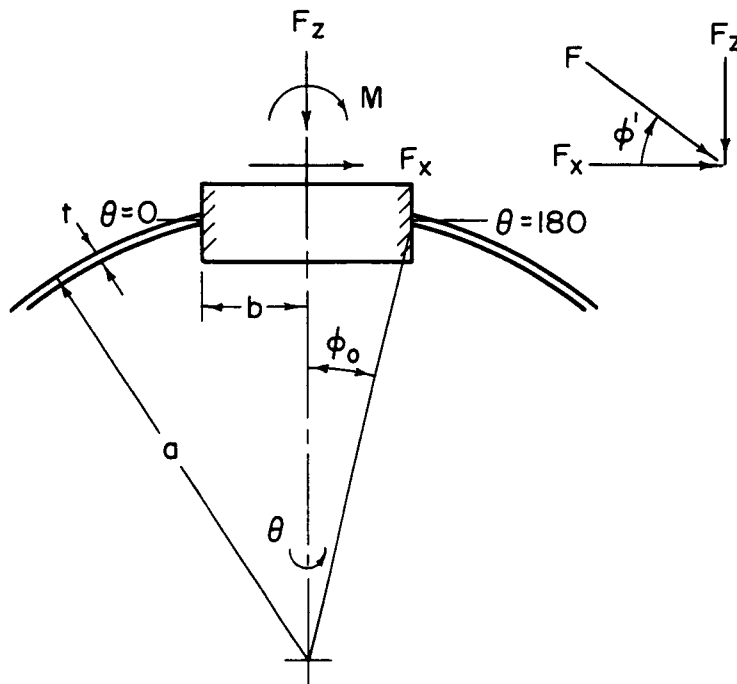The loading F_Z of Figure 7 is axisymmetric. The other loadings F_X and M are antimetric (cosine-sine variation). These loadings were analyzed by the procedures outlined in Appendix B. Calculations gave the following results:

From F_Z:

$$\text{Deflection, } w = -0.037 \times 10^{-4} F_Z$$

$$\text{Stress, } \sigma_\phi = \mp 6.24 F_Z - 8.90 F_Z \tag{20}$$

$$\text{Stress, } \sigma_\theta = \pm 0.864 F_Z + 2.94 F_Z.$$

From F_X for $\theta = 0$ degrees:

$$\text{Deflection, } w = -0.79 \times 10^{-6} F_X$$

$$\text{Stress, } \sigma_\phi = \pm 3.78 F_X + 2.08 F_X \tag{21}$$

$$\text{Stress, } \sigma_\theta = \pm 1.53 F_X + 0.69 F_X$$

From M for $\theta = 0$:

$$\text{Deflection, } w = 9.27 \times 10^{-6} M$$

$$\text{Stress, } \sigma_\phi = \pm 7.90 M + 1.71 M \tag{22}$$

$$\text{Stress, } \sigma_\theta = \pm 2.43 M + 0.56 M,$$

where the upper sign on bending component of stress refers to the outside of the shell and the lower sign refers to the inside of the shell.

The relations between the deflection and stresses, and the forces F_Z and F_X and the moment M can be used to determine the critical angle ϕ' at which the deflection or the stress will be maximum. From Figure 7, if a force F acts at an angle ϕ' then:

$$F_Z = F \sin \phi'$$

$$F_X = F \cos \phi' \tag{23}$$

$$M = zF_X = 0.31 F \cos \phi'.$$

The moment M is due to F_X acting at a moment arm at the support. The distance z from the shell to the center of the bearing location was estimated at 0.31 inches max.

The deflection w and stress σ_ϕ from the three loadings add to produce maximum magnitudes at $\theta = 180$. Adding w and σ_ϕ from Equations (20), (21), and (22) for $\theta = 180$, and introducing Equation (23) gives:

$$w = -0.037 \times 10^{-4} F \sin \phi' + 0.79 \times 10^{-6} F \cos \phi'$$

$$-9.27 \times 10^{-6} (0.31) F \cos \phi'$$

and

$$\sigma_\phi = (\mp 6.24 - 8.90) \, F \sin \phi' + (\mp 3.78 - 2.08) \, F \cos \phi'$$

$$+ (\mp 2.43 - 0.56) \, 0.31 \, F \cos \phi'$$

or

$$w = -3.7 \times 10^{-6} \, F \sin \phi' - 2.09 \times 10^{-6} \, F \cos \phi'$$

(24)

$$\sigma_\phi = -15.14 \, F \sin \phi' - 6.79 \, F \cos \phi' \, ,$$

where the upper sign has been taken for the bending components of σ_ϕ. The values of ϕ' which maximize these expressions are:

$$\phi' = 60.5 \text{ degrees for maximum x}$$

(25)

$$\phi' = 65.7 \text{ degrees for maximum } \sigma_\phi \, .$$

For an inertia load P of 584 pounds [Equation (19)] attached to two supports:

$$F = \frac{1}{2} P = 297 \text{ pounds.}$$

(26)

Substituting ϕ' from Equation (25) in Equation (24) for F = 297 pounds results in:

$$\text{Maximum } w = -4.25 \, F \times 10^{-6} = -4.25 (297) \times 10^{-6} = -0.00126$$

$$\text{Maximum } \sigma_\phi = -16.59 \, F = -16.59 (297) = -4920 \text{ psi.}$$

For F in the opposite direction, the maximum deflection and stress, of course, would be opposite in sign or 0.00126 inches and 4920 pounds per square inch.

The maximum rotation, $\Delta \phi$, at a pivot would result from loadings F_x and M ($\phi = 0$). From the first of Equations (24), the corresponding deflection is:

$$w = -2.09 \times 10^{-6} \, F = -2.09 \times 10^{-6} (297)$$

$$= -0.00062 \text{ in.}$$

This deflection occurs at a radius b = 3.125 inches from the pivot and causes a $\Delta \phi$ of:

$$\Delta \phi \cong \frac{0.00062}{3.125} \cong 0.0002 \text{ radian (40 seconds)} \, .$$

Deflections and stresses at the three mounting supports were also considered. Disregarding local effects due to irregularities in shape of the supports, it was estimated that deflections and stress would be lower than those calculated above for the trunnion supports.

A 10-pound resolver is also attached to the frame. Although it is of low weight, it has a large moment arm which causes considerable bending. Bending stresses of about ±2000 psi were estimated.

The natural frequency of the frame was estimated by inextensional theory (bending without stretching of the middle surface). This theory has been shown to be conservative. The calculations described in Appendix B showed that the frequency of the lowest normal mode would be:

$$f = 79.3 \frac{t}{a^2} \sqrt{\frac{E(1-\mu)}{\rho}} .$$

For an aluminum shell with t = 0.05 inch and a = 9.75 inches the estimated frequency is:

$$f = 350 \text{ cycles per second }.$$

This frequency is sufficiently high that very little effect on the system frequency would be expected.

The above analyses of deflection, stresses, and frequency in the frame have been greatly simplified. Stiffening effects of the flanges and other local reinforcements have been neglected. Because of this added stiffness, the deflections and stresses, in general should be lower and the frequency should be higher than the calculated values presented. The simplified analyses should be considered conservative. Theoretical results should be confirmed by experiment. This is the emphasis of the work now under way.

DESIGN SYNTHESIS USING A DIGITAL COMPUTER

Mathematical Analysis

The approach used in the analysis of gimbal rings is based on the stiffness-matrix method. This method was designed to permit the analysis of complicated, highly redundant structures. However, it was particularly useful for the present problem, since both the analysis of the stresses and the calculation of the frequency of the vibration of each ring could be carried out with this method.

The stiffness-matrix method is applied to calculating the deflection and stresses in the nonuniform ring in the following way. The ring is assumed to be broken up into a number of short segments. These segments are short enough so that, to a good approximation, they may be considered as straight beams. Now from simple beam theory, it is possible to write a set of 12 equations relating the forces and moments on each end of the beam to the deflections of each end of the beam. In the matrix equation:

$$\vec{F}_i = K_i \vec{u}_i$$

$\vec{F}$ and $\vec{u}$ are the 12 fold force and displacement vectors respectively, and K is the 12 x 12 "stiffness matrix" for the beam segment. In the inverse equation:

$$\vec{u}_i = K_i^* \vec{F}_i \ ,$$

the matrix K_i^* is called the "flexibility matrix". It is apparent that K_i^* is the inverse of K_i.

The stiffness-matrix approach consists of appropriately combining the stiffness matrices of each beam element to obtain a stiffness matrix for the entire ring. Then

$$\vec{F} = K \vec{u} \ ,$$

where F is the set of loads and moments applied to the ring at the points at which the segments are joined (hereafter these points will be called "nodes") and $\vec{u}$ is the vector of displacements of the node points. K is the over-all stiffness matrix of the ring. In general K will be of the order of six times the number of node points (less the number of physical constraints put on the system).

In calculating the frequency of the free vibrations of the ring, the stiffness matrix is a part of the matrix equation:

$$M \ddot{u} + K u = 0 \ ,$$

where M is the mass matrix of the system. (All the masses are assumed to be concentrated at the nodal points.)

This section of the report gives an outline of construction of the stiffness matrix starting with the derivation of the stiffness matrix of a simple beam.

Since the beam segments are short, the contribution of shear deflection to the bending of the beam will be included. The rotational inertia term was neglected. (The results obtained for the frequencies of vibration may be a little high because of this assumption.)

The vector representation of the components of the forces, moments, displacements, and rotations is shown in Figure 8. The vector quantities are assumed positive if they lie in the positive direction of the corresponding axes. (The right-hand rule is assumed for the vector representation of the moments and displacements.)

The notation I_x and I_z will be used for the moments of inertia of the cross section of the beam relative to the x and z axes respectively, S is the torsional rigidity of the beam, A is the cross-sectional area, G the modulus of rigidity, E is Young's modulus, and L is the length of the beam segment. The ends of the beam segment are numbered 1 and 2. The forces, moments, and displacements are given subscripts 1 and 2 (as in Figure 8) referring to the end of the beam to which they correspond.

Suppose Point 2 is deflected in the z direction by the amount w_2 with the accompanying α_2 rotation, keeping the displacement in the other directions zero (including all displacements at Point 1).

Then by Castigliano's theorem the strain energy of the beam is given by:

$$U = \int_0^L \frac{(M_{x2} + F_{z2} y)^2}{2EI_x} \, dy + \int_0^L \frac{F_{z2}^2}{2AG} \, dy \, .$$

(The second term represents the so-called "shear deflection" of the beam).

The deflection of Point 2 in the z direction is then given by:

$$w_2 = \frac{\partial U}{\partial F_{z2}} = \int_0^L \frac{(M_{x2} + F_{z2} y)y}{EI_x} dy + \int_0^L \frac{F_{z2}}{AG} \, dy \, .$$

Assuming that the cross section of the beam segment is uniform:

$$w_2 = \frac{M_{x2}L^2}{2EI_x} + \frac{F_{z2}L^3}{3EI_x} + \frac{F_{z2}L}{AG} \, ;$$

similarly

$$\alpha_2 = \frac{\partial U}{\partial M_{x2}} = \frac{M_{x2}L}{EI_x} + \frac{F_{z2}L^2}{2EI_x} \, .$$
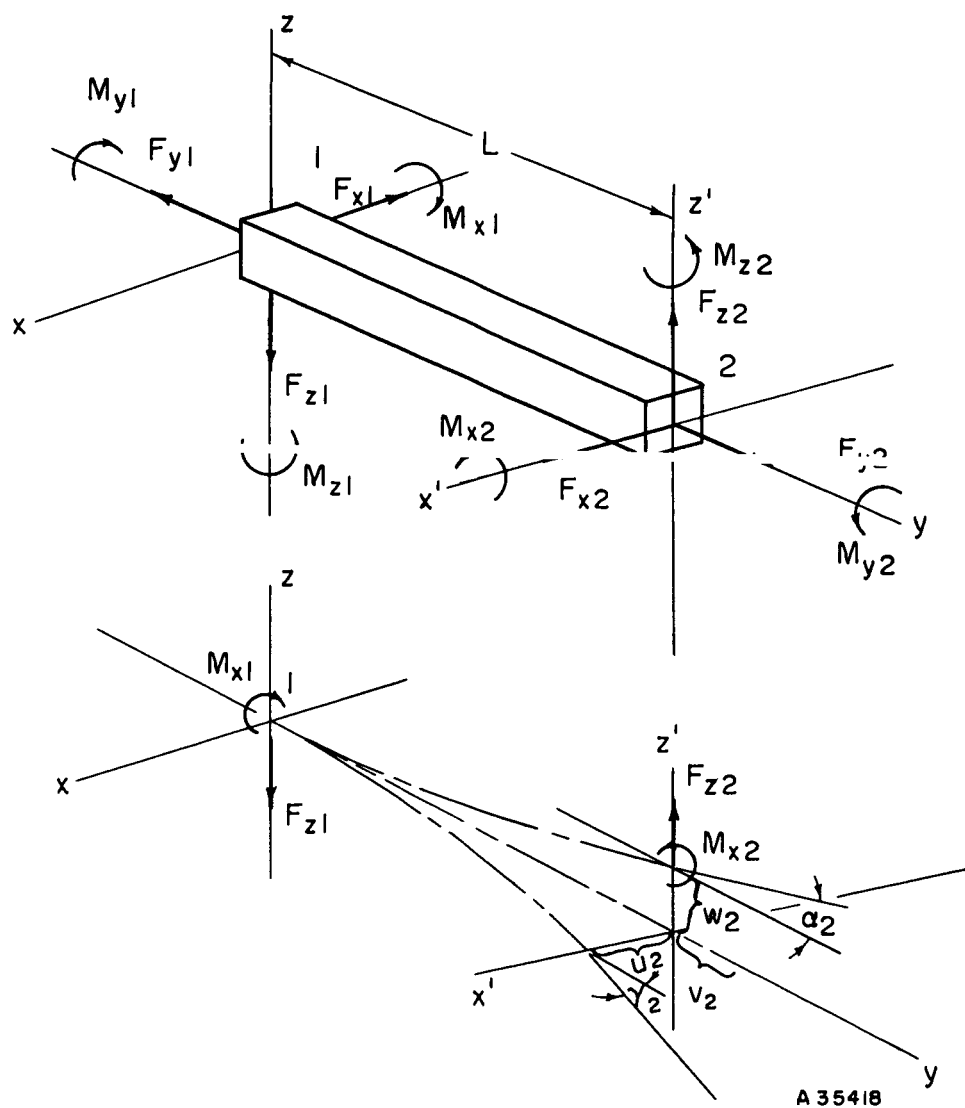
FIGURE 8. FORCES ACTING ON BEAM 1-2

Writing these two equations in matrix form gives:

$$\begin{bmatrix} w_2 \\ \alpha_2 \end{bmatrix} = \begin{bmatrix} \dfrac{L^3}{3I_x} + \dfrac{L}{AG} & \dfrac{L^2}{2EI_x} \\ \dfrac{L^2}{2EI_x} & \dfrac{L}{EI_x} \end{bmatrix} \begin{bmatrix} F_{z2} \\ M_{x2} \end{bmatrix}$$

The 2 x 2 matrix is the flexibility matrix for this particular deformation. Solving for the forces (i.e., inverting the flexibility matrix) gives:

$$\begin{bmatrix} F_{z2} \\ M_{x2} \end{bmatrix} = \frac{1}{Q} \begin{bmatrix} 1 & -\dfrac{L}{2} \\ -\dfrac{L}{2} & \dfrac{L^2}{3} + \dfrac{EI_x}{AG} \end{bmatrix} \begin{bmatrix} w_2 \\ \alpha_2 \end{bmatrix} \qquad (27)$$

where $Q = \dfrac{L^3}{12EI_x} + \dfrac{L}{AG}$. Now by equilibrium considerations, $F_{z1} = -F_{z2}$ and $M_{x1} = -M_{x2} - LF_{z2}$ or in matrix form:

$$\begin{bmatrix} F_{z1} \\ M_{x1} \end{bmatrix} = \begin{bmatrix} -1 & 0 \\ -L & -1 \end{bmatrix} \begin{bmatrix} F_{z2} \\ M_{x2} \end{bmatrix} \qquad (28)$$

Substituting this in Equation (27) gives:

$$\begin{bmatrix} F_{z1} \\ M_{x1} \end{bmatrix} = \frac{1}{Q} \begin{bmatrix} -1 & 0 \\ -L & -1 \end{bmatrix} \begin{bmatrix} 1 & -\dfrac{L}{2} \\ -\dfrac{L}{2} & \dfrac{L^2}{3} + \dfrac{EI_x}{AG} \end{bmatrix} \begin{bmatrix} w_2 \\ \alpha_2 \end{bmatrix}$$

$$= \frac{1}{Q} \begin{bmatrix} -1 & \dfrac{L}{2} \\ -\dfrac{L}{2} & \dfrac{L^2}{6} - \dfrac{EI_x}{AG} \end{bmatrix} \begin{bmatrix} w_2 \\ \alpha_2 \end{bmatrix} ; \qquad (29)$$

similarly for a u_2 and γ_2 displacement:

$$\begin{bmatrix} F_{x2} \\ M_{z2} \end{bmatrix} = \frac{1}{R} \begin{bmatrix} 1 & \dfrac{L}{2} \\ \dfrac{L}{2} & \dfrac{L^2}{3} + \dfrac{EI_z}{AG} \end{bmatrix} \begin{bmatrix} u_2 \\ \gamma_2 \end{bmatrix} , \qquad (30)$$

where $R = \dfrac{L^3}{12EI_z} + \dfrac{L}{AG}$.

Again for equilibrium of the beam it is necessary that:

$$F_{x1} = -F_{x2} \qquad M_{z1} = -M_{z2} + L F_{x2},$$

or in matrix form

$$
\begin{bmatrix} F_{x1} \\ M_{z1} \end{bmatrix}
=
\begin{bmatrix} -1 & 0 \\ L & -1 \end{bmatrix}
\begin{bmatrix} F_{x2} \\ M_{z2} \end{bmatrix} .
\tag{31}
$$

For a v_2 displacement,

$$v_2 = \frac{F_{y2} L}{AE}$$

or

$$F_{y2} = \frac{AE}{L} v_2 = -F_{y1} .$$

(32)

For a rotation β_2,

$$M_{y2} = \frac{1}{S} \beta_2 \tag{33}$$

or

$$\beta_2 = S M_{y2} = -S M_{y1} . \tag{34}$$

The results obtained so far can be combined into two matrix equations. Combining from Equations (27), (30), (32), and (34) gives:

$$
\begin{bmatrix} F_{x2} \\ F_{y2} \\ F_{z2} \\ M_{x2} \\ M_{y2} \\ M_{z2} \end{bmatrix}
=
\begin{bmatrix}
\frac{1}{R} & 0 & 0 & 0 & 0 & \frac{L}{2R} \\
0 & \frac{AE}{L} & 0 & 0 & 0 & 0 \\
0 & 0 & \frac{1}{Q} & -\frac{L}{2Q} & 0 & 0 \\
0 & 0 & -\frac{L}{2Q} & \frac{L^2}{3Q}+\frac{EI_x}{QAG} & 0 & 0 \\
0 & 0 & 0 & 0 & S & 0 \\
\frac{L}{2R} & 0 & 0 & 0 & 0 & \frac{L^2}{3R}+\frac{EI_z}{QAG}
\end{bmatrix}
\begin{bmatrix} u_2 \\ v_2 \\ w_2 \\ \alpha_2 \\ \beta_2 \\ \gamma_2 \end{bmatrix}
\tag{35}
$$

which can be abbreviated as:

$$\vec{F}_2 = K_{22} \vec{u}_2 . \tag{36}$$

From Equations (28), (31), (32), and (34), the following matrix relation between the forces forces can be obtained:

$$
\begin{bmatrix} F_{x1} \\ F_{y1} \\ F_{z1} \\ M_{x1} \\ M_{y1} \\ M_{z1} \end{bmatrix} = \begin{bmatrix} -1 & 0 & 0 & 0 & 0 & 0 \\ 0 & -1 & 0 & 0 & 0 & 0 \\ 0 & 0 & -1 & 0 & 0 & 0 \\ 0 & 0 & -L & -1 & 0 & 0 \\ 0 & 0 & 0 & 0 & -1 & 0 \\ L & 0 & 0 & 0 & 0 & -1 \end{bmatrix} \begin{bmatrix} F_{x2} \\ F_{y2} \\ F_{z2} \\ M_{x2} \\ M_{y2} \\ M_{z2} \end{bmatrix} , \tag{37}
$$

which is abbreviated as:

$$\vec{F}_1 = B_{21} \vec{F}_2 . \tag{38}$$

Combining Equations (36) and (38) gives:

$$\vec{F}_1 = B_{21} K_{22} \vec{u}_2 \tag{39}$$

or

$$\vec{F}_1 = K_{21} \vec{u}_2 \tag{40}$$

where K_{21} is the matrix product $B_{21}K_{22}$. By carrying out this multiplication it can be shown that:

$$
\begin{bmatrix} F_{x1} \\ F_{y1} \\ F_{z1} \\ M_{x1} \\ M_{y1} \\ M_{z1} \end{bmatrix} = \begin{bmatrix} -\dfrac{1}{R} & 0 & 0 & 0 & 0 & -\dfrac{L}{2R} \\ 0 & -\dfrac{AE}{L} & 0 & 0 & 0 & 0 \\ 0 & 0 & -\dfrac{1}{Q} & \dfrac{L}{2Q} & 0 & 0 \\ 0 & 0 & -\dfrac{L}{2Q} & \dfrac{L^2}{6Q} - \dfrac{EI_x}{QAG} & 0 & 0 \\ 0 & 0 & 0 & 0 & -S & 0 \\ \dfrac{L}{2R} & 0 & 0 & 0 & 0 & \dfrac{L^2}{6R} - \dfrac{EI_z}{QAG} \end{bmatrix} \begin{bmatrix} u_2 \\ v_2 \\ w_2 \\ \alpha_2 \\ \beta_2 \\ \gamma_2 \end{bmatrix} . \tag{41}
$$

It is necessary also to use the matrix equation relating the forces at Point 2 resulting from deflections at Point 1 which will be written as:

$$\vec{F}_2 = K_{12} \vec{u}_1 . \tag{42}$$

From the theorem of reciprocity, it is known that $K_{12} = K_{21}^T$ where K_{21}^T indicates the transpose of K_{21}.

This also may be verified by considering the forces and moments acting in Figure (8) as was done in deriving Equations (35) and (41).

From Equations (39) and (40), $K_{21} = B_{21} K_{22}$ so that:

$$\vec{F}_2 = (B_{21} K_{22})^T \vec{u}_1$$

or

$$\vec{F}_2 = K_{22} B_{21}^T \vec{u}_1 \quad , \tag{43}$$

since K_{22} is symmetric. From Equation (38),

$$\vec{F}_1 = B_{21} \vec{F}_2;$$

substituting this in Equation (43) gives:

$$F_1 = B_{21} K_{22} B_{21}^T \vec{u}_1 \quad . \tag{44}$$

This gives all the matrix relations between the deformations and forces at both ends of the beam. Equations (36), (39), (43), and (44) can be written in the combined matrix form:

$$\begin{bmatrix} \vec{F}_1 \\ \vec{F}_2 \end{bmatrix} = \begin{bmatrix} K_{11} & K_{12} \\ K_{21} & K_{22} \end{bmatrix} \begin{bmatrix} \vec{u}_1 \\ \vec{u}_2 \end{bmatrix} \quad , \tag{45}$$

where $\vec{F}_1$, $\vec{F}_2$, $\vec{u}_1$, and $\vec{u}_2$ are sixfold vectors, and K_{ij} are 6 x 6 matrices. K_{22} is shown in Equation (35) and the other three matrices are calculated from K_{22} from the relations:

$$K_{21} = B_{21} K_{22} \quad ,$$

$$K_{12} = K_{21}^T = K_{22} B_{21}^T \quad ,$$

and

$$K_{11} = B_{21} K_{22} B_{21}^T \quad .$$

The matrix B_{21} is shown in Equation (37).

The matrices K_{21}, K_{12}, and K_{11} could have been derived from a consideration of the appropriate forces and deflections of the beam itself as was done in deriving K_{22}. The approach used above was chosen to show how the full 12 x 12 stiffness matrix for a beam could be derived using the two 6 x 6 matrices K_{22} and B_{12}. This approach simplifies the work of programming the calculations for a computing machine.

Now suppose this beam is part of a larger structure. In order to combine the deflections and forces for the various beams that make up the structure, it is necessary to express all of these deflections and forces in the same coordinate system. This is accomplished by multiplying the forces and deflections by the rotation matrix, obtained as follows:

Consider two coordinate systems shown below:
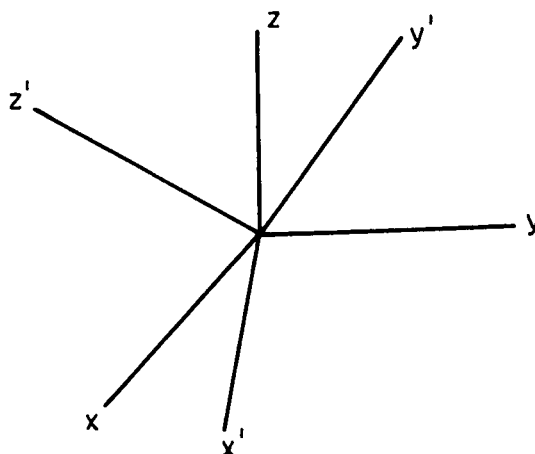
It is known that the components of a vector in the x', y', z' coordinate system are related to the components of the same vector in the (x, y, z) coordinate system by the relation:

$$
\begin{bmatrix} x \\ y \\ z \end{bmatrix} = \begin{bmatrix} l_{x'x} & l_{x'y} & l_{x'z} \\ l_{y'x} & l_{y'y} & l_{y'z} \\ l_{z'x} & l_{z'y} & l_{z'z} \end{bmatrix} \begin{bmatrix} x' \\ y' \\ z' \end{bmatrix} , \tag{46}
$$

where l_{ij} is the cosine of the angle between the axes indicated by the subscripts. Thus

$$
\begin{bmatrix} F_{x1} \\ F_{y1} \\ F_{z1} \end{bmatrix} = \begin{bmatrix} l_{x'x} & l_{x'y} & l_{x'z} \\ l_{y'x} & l_{y'y} & l_{y'z} \\ l_{z'x} & l_{z'y} & l_{z'z} \end{bmatrix} \begin{bmatrix} F_{x'1} \\ F_{y'1} \\ F_{z'1} \end{bmatrix} ,
$$

where $(F_{x'1}, F_{y'1}, F_{z'1})$ are the components of the force vector F_1 in the over-all coordinate system of the structure. Similarly

$$
\begin{bmatrix} M_{x1} \\ M_{y1} \\ M_{z1} \end{bmatrix} = \begin{bmatrix} l_{x'x} & l_{x'y} & l_{x'z} \\ l_{y'x} & l_{y'y} & l_{y'z} \\ l_{z'x} & l_{z'y} & l_{z'z} \end{bmatrix} \begin{bmatrix} M_{x'1} \\ M_{y'1} \\ M_{z'1} \end{bmatrix} .
$$

Combining these last two equations for the sixfold vector $\vec{F}_1$ and $\vec{F}_1'$ gives the relation:

$$\vec{F}_1 = R \, \vec{F}_1' , \tag{47}$$

where

$$R = \begin{bmatrix} l_{x'x} & l_{x'y} & l_{x'z} & 0 & 0 & 0 \\ l_{y'x} & l_{y'y} & l_{y'z} & 0 & 0 & 0 \\ l_{z'x} & l_{z'y} & l_{z'z} & 0 & 0 & 0 \\ 0 & 0 & 0 & l_{x'x} & l_{x'y} & l_{x'z} \\ 0 & 0 & 0 & l_{y'x} & l_{y'y} & l_{y'z} \\ 0 & 0 & 0 & l_{z'x} & l_{z'y} & l_{z'z} \end{bmatrix} .$$

The same rotation relation holds between the other sixfold force and displacement vectors referred to the beam and structure coordinates, that is,

$$\vec{F}_2 = R \, \vec{F}_2' ,$$

$$\vec{u}_1 = R \, \vec{u}_1' ,$$

$$\vec{u}_2 = R \, \vec{u}_2' .$$

Thus, Equations (36), (39), (43), and (44) can be written in terms of the structure coordinates as:

$$R \, \vec{F}_2' = K_{22} \, R \, \vec{u}_2' ,$$

$$R \, \vec{F}_1' = B_{21} \, K_{22} \, R \, \vec{u}_2' ,$$

$$R \, \vec{F}_2' = K_{22} \, B_{21}^T \, R \, \vec{u}_1' ,$$

$$R \, \vec{F}_1' = B_{21} \, K_{22} \, B_{21}^T \, R \, \vec{u}_1' . \tag{48}$$

The rotation matrix has the property that

$$R^T = R^{-1} .$$

Thus, premultiplying both sides of Equation (48) by R^T gives:

$$\vec{F}_2' = R^T \, K_{22} \, R \, \vec{u}_2' ,$$

$$\vec{F}_1' = R^T \, B_{21} \, K_{22} \, R \, \vec{u}_2' ,$$

$$\vec{F}_2' = R^T \, K_{22} \, B_{21}^T \, R \, \vec{u}_1' ,$$

$$\vec{F}_1' = R^T \, B_{21} \, K_{22} \, B_{21}^T \, R \, \vec{u}_1' . \tag{49}$$

In the coordinate system of the structure, the analogue of Equation (45) is then:

$$\begin{bmatrix} \vec{F}'_1 \\ \vec{F}'_2 \end{bmatrix} = \begin{bmatrix} K'_{11} & K'_{12} \\ K'_{21} & K'_{22} \end{bmatrix} \begin{bmatrix} \vec{u}'_1 \\ \vec{u}'_2 \end{bmatrix}, \tag{50}$$

where

$$K'_{11} = R^T B_{21} K_{22} B_{21}^T R,$$

$$K'_{12} = R^T K_{22} B_{21}^T R$$

$$K'_{21} = R^T B_{21} K_{22} R$$

$$K'_{22} = R^T K_{22} R .$$

Equation (50) gives the matrix equation between the displacements and forces at two ends of a beam when these displacements and forces are related to the coordinate system of the over-all structure. The matrix

$$\begin{bmatrix} K'_{11} & K'_{12} \\ K'_{21} & K'_{22} \end{bmatrix}$$

will be called the stiffness matrix for the Beam (1,2). Once the stiffness matrices are calculated for each beam of the structure, it is necessary to combine these matrices in the proper way to represent the structure as a whole. The way that this is done can be illustrated by the two-member beam shown below.
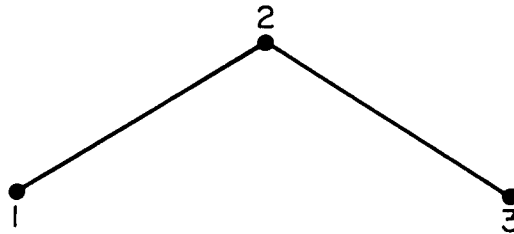
Calculating the stiffness matrix of Beam (1,2) gives, as in Equation (50):

$$\begin{bmatrix} F'_1 \\ F'_2 \end{bmatrix} = \begin{bmatrix} K'_{11} & K'_{12} \\ K'_{21} & K'_{22} \end{bmatrix} \begin{bmatrix} u'_1 \\ u'_2 \end{bmatrix} .$$

For Beam (2,3), the analogous matrix equation is:

$$\begin{bmatrix} F''_2 \\ F''_3 \end{bmatrix} = \begin{bmatrix} K''_{22} & K''_{23} \\ K''_{32} & K''_{33} \end{bmatrix} \begin{bmatrix} u''_2 \\ u''_3 \end{bmatrix} .$$

For the two-member frame taken as a unit, the displacements u_2'' must be equal to u_2'. The total forces acting at Point 2 must be the sum of F_2' and F_2''. Thus the matrix equation for the composite beam is:

$$\begin{bmatrix} \vec{F}_1' \\ F_2' + F_2'' \\ F_3' \end{bmatrix} = \begin{bmatrix} K_{11}' & K_{12}' & 0 \\ K_{21}' & K_{22}' + K_{22}'' & K_{23}'' \\ 0 & K_{32}'' & K_{33}'' \end{bmatrix} \begin{bmatrix} \vec{u}_1' \\ \vec{u}_2' \\ \vec{u}_3' \end{bmatrix} .$$

This result can be easily generalized to more complex structures. It can be seen that, for a given nodal point i of the structure, the submatrix K_{ii} of the over-all stiffness matrix will have added into it, one submatrix from each of the beams joined to the point i. The submatrices K_{ij} and K_{ji} will be unique since there is only one beam connecting the point i to the point j. (If there is no beam between i and j, $K_{ij} = K_{ji} = 0$.)

The rules for forming the stiffness matrix for a structure may be summarized as follows:

(1) Divide the structure up into a set of beams connected at nodal points.

(2) Number the nodal points consecutively from 1 to n.

(3) Partition the over-all 6n x 6n stiffness matrix into 6 x 6 submatrices.

(4) Calculate the basic 6 x 6 stiffness matrix of the beam connecting the ith to the jth node according to Equation (35).

(5) Calculate the matrices B and R for the Beam (i,j) by Equations (37) and (47).

(6) Calculate the four submatrices K_{ii}', K_{ij}', K_{ji}', and K_{jj}' for the Beam (i,j) from Equation (50).

(7) Add the submatrices K_{ii}' and K_{jj}' into the (i,i) and (j,j) submatrices, respectively, of the over-all stiffness matrix.

(8) Store the submatrices K_{ij}' and K_{ji}' in the (i,j) and (j,i) submatrix slots of the over-all stiffness matrix.

(9) Perform Steps (4) through (8) for all of the beams of the structure.

These operations give the stiffness matrix relating the forces and deflections of the complete structure according to the relation:

$$\vec{F} = K \vec{u} ,$$

where $\vec{F}$ is the 6n-fold vector of the external loads applied at the n nodes of the structure and $\vec{u}$ is the 6n-fold vector of the displacements of the nodes of the structure. K is the 6n x 6n stiffness matrix of the structure. (It is necessary to apply a sufficient number of constraints on the frame to keep it from moving as a rigid body. If these constraints consist of setting some components of the displacement vector equal to zero, the

corresponding rows and columns of the stiffness matrix are omitted. The remaining discussion will refer to such a "reduced" stiffness matrix.)

If the external loads on the structure are known and it is desired to find the displacements of the nodes of the structure, it is necessary to invert the reduced stiffness matrix to obtain:

$$\vec{u} = K^{-1} \vec{F} \ . \tag{51}$$

The process of inverting K is a standard matrix operation that is easily performed on a computer.

A computer program was written to implement the construction of the stiffness-matrix calculation. Briefly, this program formed the stiffness matrix from input specifying the numbers and location of the nodes of the structure, the orientation of the beams connecting the nodes, and the geometrical parameters of each beam such as A, I_x, I_y, etc., which enter the stiffness matrix in Equation (35).

From the input data, the computer program automatically sets up the stiffness matrix and inverts it. This flexibility matrix K^{-1} can then be used as in Equation (51) to calculate the nodal displacements of the structure from one or more sets of exterior loads.

Once the displacements are calculated, the stresses in each beam segment of the structure can easily be calculated from the differences between the displacements of the two nodes which lie at its end points. Starting with the two sixfold displacement vectors $\vec{u}_i$ and $\vec{u}_j$ of the ith and jth nodes expressed in the coordinate system of the structure, the forces $\vec{F}_j$ for the Beam B_{ij} (the beam connecting the ith and jth nodes) are given by the equation:

$$\vec{F}_j = K_{jj} \ R_{ij} \ (\vec{u}_j' - \vec{u}_i'), \tag{52}$$

where R_{ij} is the rotation matrix for the Beam B_{ij} and K_{jj} is the matrix K_{22} of Equation (43) for the beam. The forces F_j as calculated by Equation (52) represent the forces applied to the jth end of B_{ij} with the ith end built in (i.e., the $\vec{F}_j$ correspond to forces applied to the free end of a cantilever beam).

The stresses at any point of the beam are calculated from $\vec{F}_j$ using elementary beam theory.

A subroutine was written to have the digital computer perform the calculation of stresses in the frame members from the displacement vector $\vec{u}$ once it had been obtained.

It was mentioned at the beginning of this section that the stiffness matrix could be used to calculate the frequencies of a vibrating frame. In this approach to the vibration problem, the frame is considered to be a multiple degree of freedom system with all of the mass concentrated at the nodes. The stiffness matrix represents the aggregate of all of the springs (beams) connecting the masses. The frequency equation for free vibrations of this system is then:

$$M \ddot{u} + K u = 0,$$

where $\ddot{u}$ is the acceleration vector of all the nodes and M is the matrix of the masses associated with each node. (M is a diagonal matrix.) For harmonic motion $\ddot{u} = \omega^2 u$ so that the frequency equation is:

$$(\omega^2 u - K) u = 0 .$$

The frequencies of the modes of vibration of the structure are thus the solutions for ω^2 that make the matrix $(\omega^2 u - K)$ singular*. This is the eigenvalue problem of matrix theory. The solution of this problem was obtained also with a computer program.

The actual solutions obtained for the stresses and frequencies of the gimbal rings are reported elsewhere in this report.

Analysis of Computer Output Data

The data generated by the computer consisted of the following:

(1) Displacements and rotations at the 24 node points for each force vector considered

(2) Membrane, bending and shearing stresses, and various combinations of these stresses, at the 24 node points for each force vector considered

(3) The lowest response frequency of the gimbal for each mass vector considered.

The analysis consisted of plotting the stresses and deflections for each acceleration vector and modifying the section where necessary. A new set of input data resulted from this analysis and was used for the next iteration. At points where the stresses were too high, the section modulus was increased, and at points of low stress the section modulus was decreased. This process was repeated until the design proposed in the drawings attached was reached. The stresses and deflections for an 8-g linear acceleration in this design is shown in Appendix C.

REFERENCES

(1) Hughel, T. J., "Beryllium — A Space Age Metal", Metals Eng., Quarterly, 2 (2) (May, 1962).

(2) Seely, F. B., and Smith, J. O., Advanced Mechanics of Materials, Second Edition, John Wiley and Sons, Inc., New York (1957).

(3) DMIC Report 106, "Beryllium for Structural Applications", August, 1958, Defense Metals Information Center, Battelle Memorial Institute, Columbus, Ohio.

*The reduced stiffness matrix K used in the frequency equation also reflects the external constraints put on the system to keep it from moving as a rigid body If these constraints are properly applied, K will be nonsingular.

(4) Roark, R. J. , Formulas for Stress and Strain, Third Edition, McGraw Hill Book Company, Inc. , New York (1954).

(5) Flügge, Wilhelm, Stresses in Shells, Springer-Verlag, Berlin/Gottingen/ Heidelberg (1960).

(6) Gerdeen, J. C. , "Analysis of Shallow Spherical Shells of Circular Ring Plan Form", Masters Thesis, The Ohio State University (1962).

(7) Steele, C. R. , "Nonsymmetric Deformation of Dome-Shaped Shells of Revolution", J. Appl. Mech., 29 (2), Series E, 353-361 (June, 1962).

(8) Lowell, H. H. , "Tables of the Bessel-Kelvin Functions, ber, bei, ker, kei, and Their Derivatives for the Argument Range 0 (0.01) 107.50", NASA TR R-32 (1959).

(9) Lord Rayleigh, "On the Infinitesimal Bending of Surfaces of Revolution", Proc. London Math. Soc. , London, England, 13, 4-16 (1881).

(10) Novozhilov, V. V. , The Theory of Thin Shells, P. Noordhoff, Ltd. , The Netherlands (1959).

(11) Naghdi, P. M. , and Kalnins, A. , "On Vibrations of Elastic Spherical Shells", J. Appl. Mech. , 29 (1), Series E, 65-72 (March, 1962).

APPENDIX A

GENERALIZED EQUATIONS FOR RINGS
OF CONSTANT CROSS-SECTION

A = Area of section

S_r = Section modulus about r axis

S_z = Section modulus about z axis

Element A
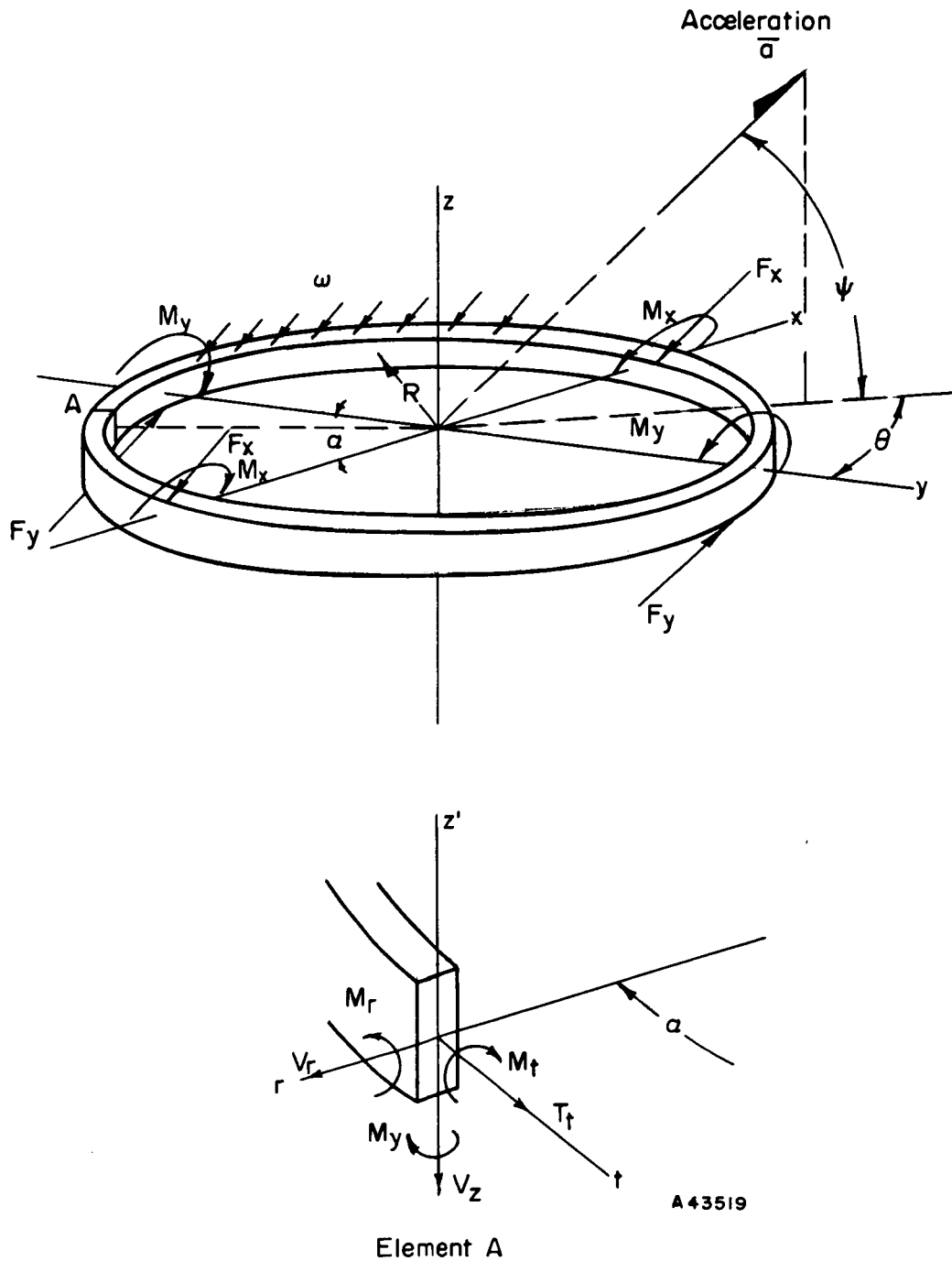
FIGURE A-1. GENERALIZED LOADING CONDITIONS FOR RING SUBJECTED TO INERTIAL FORCES
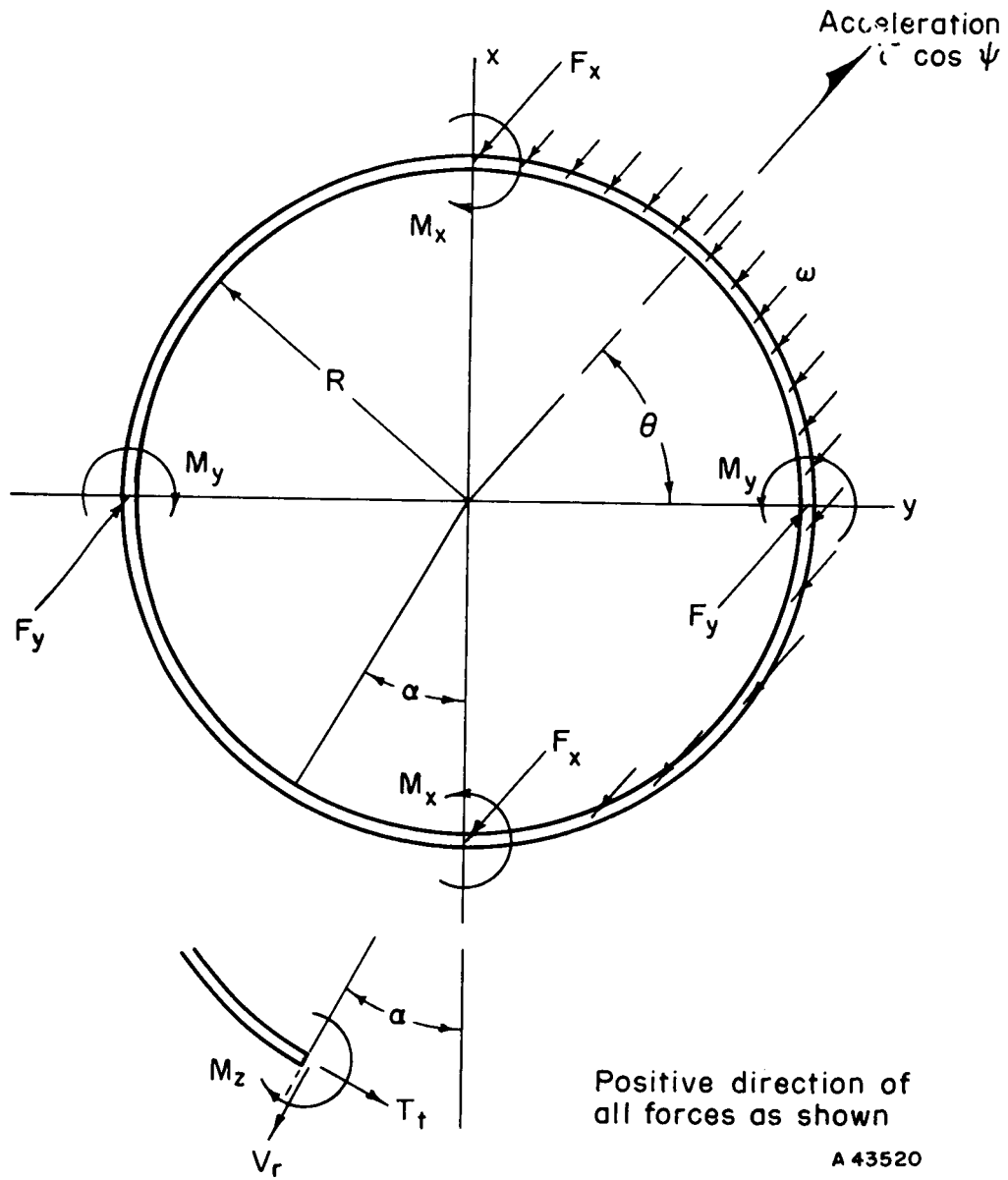
FIGURE A-2. INERTIAL FORCES DUE TO ACCELERATION IN PLANE OF RING

TABLE A-1. EQUATIONS FOR M_z

Location (α), degrees	M_z	
	x sin Θ cos Ψ	x cos Θ cos Ψ
0-$\triangle\alpha$	$-0.182F_xR-0.071\omega R^2+0.137M_y$	$+0.500M_x$
0+$\triangle\alpha$	$-0.182F_xR-0.071\omega R^2+0.137M_y$	$-0.500M_x$
15	$-0.063F_xR-0.053\omega R^2+0.115M_y$	$-0.066F_xR-0.126\omega R^2-0.335M_x$
30	$+0.026F_xR-0.009\omega R^2+0.052M_y$	$-0.093F_xR-0.206\omega R^2-0.182M_x$
45	$+0.079F_xR+0.037\omega R^2-0.050M_y$	$-0.079F_xR-0.205\omega R^2-0.050M_x$
60	$+0.093F_xR+0.085\omega R^2-0.182M_y$	$-0.026F_xR-0.092\omega R^2-0.052M_x$
75	$+0.066F_xR+0.079\omega R^2-0.335M_y$	$+0.063F_xR+0.145\omega R^2+0.115M_x$
90-$\triangle\alpha$	$-0.500M_y$	$+0.182F_xR+0.500\omega R^2+0.137M_x$
90+$\triangle\alpha$	$+0.500M_y$	$+0.182F_xR+0.500\omega R^2+0.137M_x$

TABLE A-2. EQUATIONS FOR T_t

Location (α), degrees	T_t	
	x sin Θ cos Ψ	x cos Θ cos Ψ
0-$\triangle\alpha$	$+0.318F_x+0.500\omega R+0.637\dfrac{M_y}{R}$	$+0.500F_x$
0+$\triangle\alpha$	$+0.318F_x+0.500\omega R+0.637\dfrac{M_y}{R}$	$-0.500F_x$
15	$+0.438F_x+0.551\omega R+0.615\dfrac{M_y}{R}$	$-0.563F_x-0.385\omega R+0.165\dfrac{M_x}{R}$
30	$+0.526F_x+0.695\omega R+0.552\dfrac{M_y}{R}$	$-0.593F_x-0.706\omega R+0.318\dfrac{M_x}{R}$
45	$-0.579F_x+0.902\omega R+0.450\dfrac{M_y}{R}$	$-0.579F_x-0.913\omega R+0.450\dfrac{M_x}{R}$
60	$+0.593F_x+1.156\omega R+0.318\dfrac{M_y}{R}$	$-0.526F_x-0.956\omega R+0.552\dfrac{M_x}{R}$
75	$+0.563F_x+1.392\omega R+0.165\dfrac{M_y}{R}$	$-0.438F_x-0.822\omega R+0.615\dfrac{M_x}{R}$
90-$\triangle\alpha$	$+0.500F_x+1.571\omega R$	$-0.318F_x-0.500\omega R+0.637\dfrac{M_x}{R}$
90+$\triangle\alpha$	$+0.500F_x+1.571\omega R$	$-0.318F_x-0.500\omega R+0.637\dfrac{M_x}{R}$

TABLE A-3. EQUATIONS FOR V_r

Location (α), degrees	V_r x sin θ cos Ψ	x cos θ cos Ψ
$0-\Delta\alpha$	$-0.500F_x$	$-0.318F_x-0.500\omega R+0.637\dfrac{M_x}{R}$
$0+\Delta\alpha$	$+0.500F_x$	$-0.318F_x-0.500\omega R+0.637\dfrac{M_x}{R}$
15	$+0.402F_x+0.123\omega R-0.165\dfrac{M_y}{R}$	$-0.179F_x-0.238\omega R+0.615\dfrac{M_x}{R}$
30	$+0.274F_x+0.203\omega R-0.318\dfrac{M_y}{R}$	$-0.026F_x-0.079\omega R+0.552\dfrac{M_x}{R}$
45	$+0.128F_x+0.201\omega R-0.450\dfrac{M_y}{R}$	$+0.128F_x+0.203\omega R+0.450\dfrac{M_x}{R}$
60	$-0.026F_x+0.090\omega R-0.552\dfrac{M_y}{R}$	$+0.274F_x+0.566\omega R+0.318\dfrac{M_x}{R}$
75	$-0.179F_x-0.145\omega R-0.615\dfrac{M_y}{R}$	$+0.402F_x+0.956\omega R+0.165\dfrac{M_x}{R}$
$90-\Delta\alpha$	$-0.318F_x-0.500\omega R-0.637\dfrac{M_y}{R}$	$+0.500F_x+1.571\omega R$
$90+\Delta\alpha$	$-0.318F_x-0.500\omega R-0.637\dfrac{M_y}{R}$	$-0.500F_x-1.571\omega R$

TABLE A-4. EQUATIONS FOR M_r

Location, (α), degrees	M_r, x sin Ψ
$0 - \Delta\alpha$	$+ 0.500\ F_x R + 0.571\ \omega R^2 + 0.500\ M_y$
$0 + \Delta\alpha$	$+ 0.500\ F_x R + 0.571\ \omega R^2 + 0.500\ M_y$
15	$+ 0.353\ F_x R + 0.518\ \omega R^2 + 0.483\ M_y + 0.130\ M_x$
30	$+ 0.183\ F_x R + 0.371\ \omega R^2 + 0.434\ M_y + 0.250\ M_x$
45	$+ 0.111\ \omega R^2 + 0.354\ M_y + 0.354\ M_x$
60	$- 0.183\ F_x R - 0.214\ \omega R^2 + 0.250\ M_y + 0.434\ M_x$
75	$- 0.353\ F_x R - 0.512\ \omega R^2 + 0.130\ M_y + 0.483\ M_x$
$90 - \Delta\alpha$	$- 0.500\ F_x R - 1.000\ \omega R^2 + 0.500\ M_x$
$90 + \Delta\alpha$	$- 0.500\ F_x R - 1.000\ \omega R^2 + 0.500\ M_x$
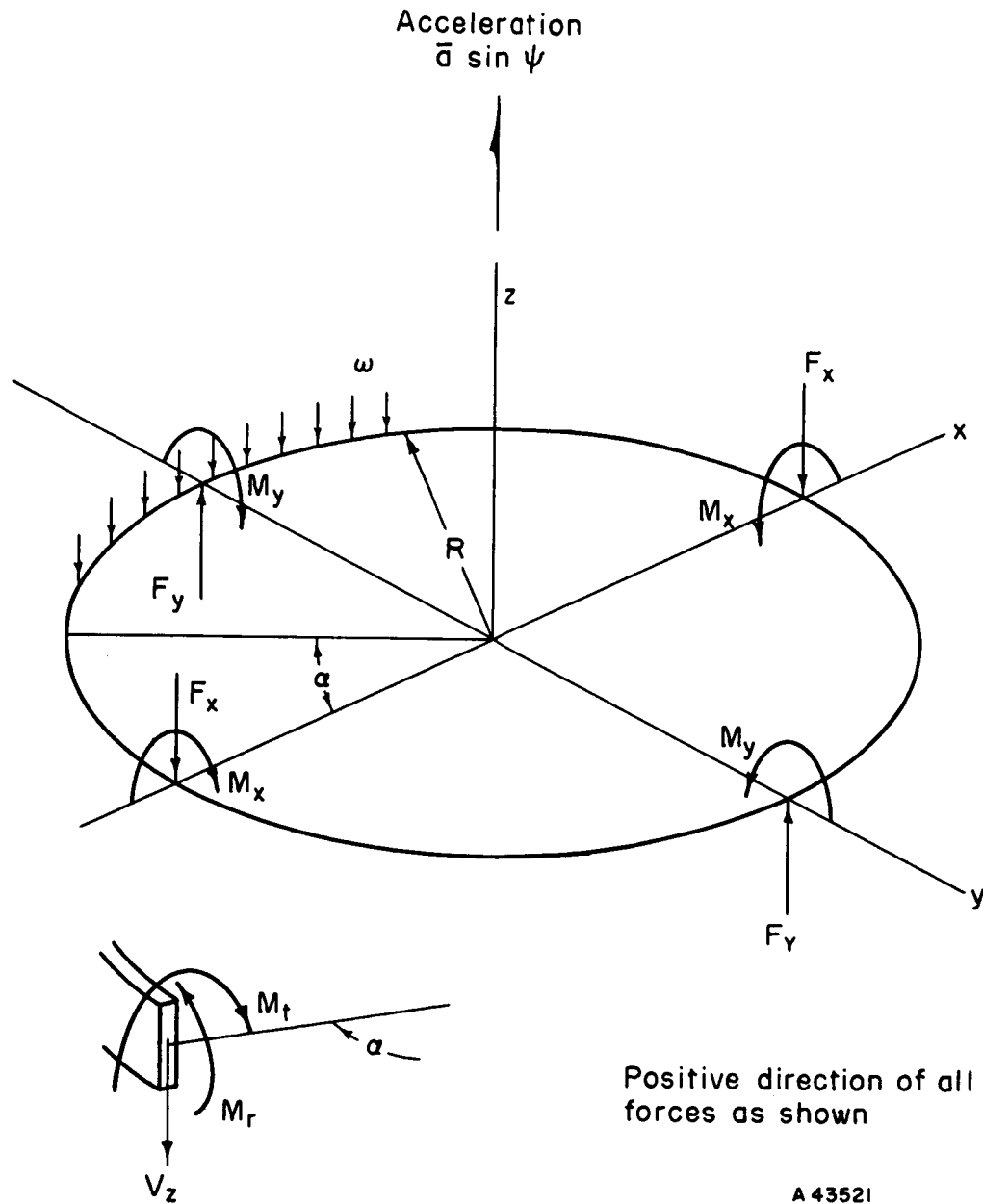
FIGURE A-3. INERTIAL FORCES DUE TO ACCELERATION
PERPENDICULAR TO PLANE OF RING

TABLE A-5. EQUATIONS FOR M_t

Location (α), degrees	M_t, x sin Ψ
$0 - \triangle \alpha$	$- 0.500\ M_x$
$0 + \triangle \alpha$	$+ 0.500\ M_x$
15	$- 0.113\ F_x R + 0.154\ \omega R^2 + 0.483\ M_x - 0.130\ M_y$
30	$- 0.183\ F_x R + 0.261\ \omega R^2 + 0.434\ M_x - 0.250\ M_y$
45	$- 0.207\ F_x R + 0.326\ \omega R^2 + 0.354\ M_x - 0.354\ M_y$
60	$- 0.183\ F_x R + 0.317\ \omega R^2 + 0.250\ M_x - 0.434\ M_y$
75	$- 0.113\ F_x R + 0.210\ \omega R^2 + 0.130\ M_x - 0.483\ M_y$
$90 - \triangle \alpha$	$- 0.500\ M_y$
$90 + \triangle \alpha$	$+ 0.500\ M_y$

TABLE A-6. EQUATIONS FOR V_z

Location (α), degrees	V_z, x sin Ψ
$0 - \triangle \alpha$	$- 0.500\ F_x$
$0 + \triangle \alpha$	$+ 0.500\ F_x$
15	$+ 0.500\ F_x + 0.262\ \omega R$
30	$+ 0.500\ F_x + 0.524\ \omega R$
45	$+ 0.500\ F_x + 0.786\ \omega R$
60	$+ 0.500\ F_x + 1.048\ \omega R$
75	$+ 0.500\ F_x + 1.310\ \omega R$
$90 - \triangle \alpha$	$+ 0.500\ F_x + 1.571\ \omega R$
$90 + \triangle \alpha$	$- 0.500\ F_x - 1.571\ \omega R$

APPENDIX B

CALCULATIONS OF FRAME STRESSES AND DEFLECTIONS

APPENDIX B

CALCULATIONS OF FRAME STRESSES AND DEFLECTIONS

The calculations of the deflections and stresses from the loadings of Figure 7 are given below. Also included is the method of calculation used to estimate the natural frequency of the frame. As stated in the body of this report, the frame together with the covers was considered to constitute a spherical shell. Thus, the calculations are based on shell theory.

Axisymmetric Loading

The effects of the axisymmetric loading F_Z of Figure 7 were found from the curves of influence numbers in Reference 6[*]. Solution of the problem is aided by the breakdown shown in Figure B-1. The pivot support is assumed to be infinitely rigid compared to the shell. Thus, the slope and the horizontal deflection at the support are zero and the boundary equations become:

$$w_b' \ (F_Z) + w_b' \ (Q_b) + w_b' \ (M_b) = 0 \tag{B-1}$$

$$\Delta_b \ (F_Z) + \Delta_b \ (Q_b) + \Delta_b \ (M_b) = 0 \ . \tag{B-2}$$
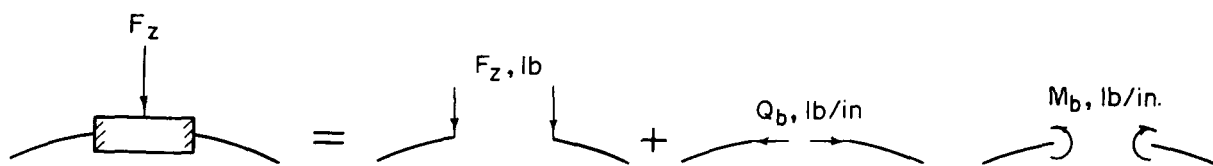
FIGURE B-1. BREAKDOWN OF PROBLEM FOR AXISYMMETRIC
F_z LOADING ON FRAME

For the parameters $b = 3.125$ inches and $\ell = 0.386$ inches, the ratio $\dfrac{b}{\ell} = \dfrac{3.125}{0.386} = 8.1 \cong 8.$
From Reference (6), Figure 10:

$$w_b' \ (F_Z) = - \frac{0.12 \ F_Z \ a}{2\pi H \ell} \ , \quad \Delta_b \ (F_Z) = - \frac{10.5 \ F_Z \ a}{2\pi b \ Et}$$

$$w_b' \ (Q_b) = \frac{0.12 \ Q_b \ b^2}{H\ell} \ , \quad \Delta_b \ (Q_b) = \left(11.5 + \frac{\mu}{2}\right) \frac{Q_b \ b}{Et} \ .$$

From Reference (6), Figure 12:

$$w_b' \ (M_b) = \frac{1.36 \ M_b \ \ell}{D} \ , \quad \Delta_b \ (M) = \frac{0.95 \ M_b \ \ell}{H} \ .$$

Where

$$D = \text{flexural rigidity} = \frac{Et^3}{12 \ (1 - \mu^2)} = 117 \ \text{lb-in.}$$

[*]References are listed on page 39.

$$\ell = \text{characteristic length} = \frac{\sqrt{at}}{4\sqrt{12(1-\mu^2)}} = 0.386 \text{ in.}$$

$$H = \text{characteristic force} = \frac{Et^2}{\sqrt{12(1-\mu^2)}} = 7650 \text{ lb.}$$

Substituting the above expressions for w_b' and Δ_b in Equations (B-1) and (B-2) gives:

$$-\frac{0.12 \, F_Z \, a}{2\pi} + 0.12 \, Q_b \, b^2 + 1.36 \, M_b \, a = 0 \tag{B-3}$$

$$-\frac{10.5 \, F_Z \, a}{2\pi b} + 11.665 \, Q_b \, b + \frac{0.95 \, b \sqrt{12(1-\mu^2)}}{t} M_b = 0 . \tag{B-4}$$

Simultaneous solution of (B-3) and (B-4) for $b = 3.125$, $a = 9.75$, and $\mu = 0.33$ yields:

$$M_b = M_\phi \text{ at } b = 0.0026 \, F_Z$$

$$Q_b = 0.129 \, F_Z .$$

From Q_b and F_Z,

$$N_\phi \text{ at } b = Q_b \cos \phi_0 - F_Z \sin \phi_0$$

$$= Q_b \cos 18.7 - F_Z \sin 18.7$$

$$= -0.4455 \, F_Z$$

$$\Delta_b = 0 \rightarrow N_\theta = \mu N_\phi = -0.147 \, F_Z .$$

From Figures 10 and 12 of Reference (5):

$$w = -\frac{0.18 \, F_Z \, a}{2\pi H} + \frac{0.18 \, Q_b}{H}^2 + \frac{0.95 \, M_b \, \ell^2}{D}$$

$$= -0.037 \times 10^{-4} \, F_Z$$

$$M_\theta = -0.14 \, M_b = -.00036 \, F_Z$$

Thus deflection $w = -0.037 \times 10^{-4} \, F_Z$,

$$\text{Stress } \sigma_\phi = \mp \frac{6M_\phi}{t^2} + \frac{N_\phi}{t} = \mp 6.24 \, F_Z - 8.90 \, F_Z$$

$$\text{Stress } \sigma_\theta = \mp \frac{6M_\theta}{t^2} + \frac{N_\theta}{t} = \mp 0.864 \, F_Z - 2.94 \, F_Z$$

Antimetric Loading

Influence coefficients for asymmetric loading not tabulated like they are for axisymmetric loadings. Therefore, the basic theories applicable to spherical shells had to be employed to derive the expressions for deflections and stresses for the antimetric loading F_X of Figure 7. Following the common approach to solution of shell

problems, the membrane theory was used to balance the external force F_X and a general theory (membrane plus bending) was used to match the boundary conditions. The general theory used was that given by Steele[7].

The loading F_X of Figure 7 is antimetric (cosine - sine variation). Thus assume:

u = deflection in θ direction = $u_1 \sin \theta$

v = deflection in ϕ direction = $v_1 \cos \theta$

w = deflection in normal direction = $w_1 \cos \theta$

N_θ = membrane force in θ direction = $N_{\theta 1} \cos \theta$

N_ϕ = membrane force in ϕ direction = $N_{\phi 1} \cos \theta$

$N_{\theta\phi}$ = membrane shear force = $N_{\theta\phi 1} \sin \theta$

M_θ = bending moment in θ direction = $M_{\theta 1} \cos \theta$

M_ϕ = bending moment in ϕ direction = $M_{\phi 1} \cos \theta$

$M_{\theta\phi}$ = twisting moment = $M_{\theta\phi 1} \sin \theta$

Q_ϕ = transverse shear force = $Q_{\phi 1} \cos \theta$.

The membrane forces which balance the external force F_X are:

$$N_{\phi 1} = - N_{\theta 1} = \frac{F_X}{a \pi \cos \phi \sin \phi} \tag{B-5}$$

$$N_{\theta\phi 1} = \frac{F_X}{a \pi \sin \phi \cos^2 \phi} \ . \tag{B-6}$$

The membrane deflections, found from an integral solution using the stress-strain relations and the above membrane forces, are:

$$u_1 = \frac{2 (1 + \mu)}{Et} \frac{F_X}{\pi} \left[\frac{1}{2} \cos \phi - \log \tan \frac{\phi}{2} - 2 \cos \phi \log \cot \phi \right] \tag{B-7}$$

$$v_1 = \frac{2 (1 + \mu)}{Et} \frac{F_X}{\pi} \left[\cos \phi \log \tan \frac{\phi}{2} + \frac{1}{2} \right] \tag{B-8}$$

$$w_1 = \frac{2 (1 + \mu)}{Et} \frac{F_X}{\pi} \left[\frac{1}{2} \csc \phi \sec \phi - \cot \phi + \sin \phi \log \tan \frac{\phi}{2} \right] \ . \tag{B-9}$$

The approximate general solution of Steele[7] for a shell with hole at the apex and closed at the other pole gives:

$$u_1 = \frac{\ell (1 + \mu) \, \Psi \, \phi}{\alpha \sin \phi} \left[C_1 \, \zeta^{-1} \, \text{kei}_1 \, \zeta - C_2 \, \zeta^{-1} \, \text{ker}_1 \, \zeta \right] \tag{B-10}$$

$$v_1 = (1 + \mu)\, \Psi\, \zeta^{-1} \left[-C_1 \, \text{kei}_1' \, \zeta + C_2 \, \text{ker}_1' \, \zeta \right] \tag{B-11}$$

$$w_1 = \Psi \left[C_1 \, \text{ker}_1 \, \zeta + C_2 \, \text{kei}_1 \, \zeta \right] \tag{B-12}$$

$$N_{\theta 1} = \frac{Et\Psi}{a} \left[C_1 \, (\text{ker}_1 \, \zeta + \zeta^{-2} \, \text{kei}_1 \, \zeta - \zeta^{-1} \, \text{kei}_1' \, \zeta) \right.$$
$$\left. + C_2 \, (\text{kei}_1 \, \zeta - \zeta^{-2} \, \text{ker}_1 \, \zeta + \zeta^{-1} \, \text{ker}_1' \, \zeta) \right] \tag{B-13}$$

$$N_{\phi 1} = \frac{Et\Psi}{a} \frac{\phi \, \cot \phi}{\sin \phi} \left[C_1 \, (\zeta^{-1} \, \text{kei}_1' \zeta - \zeta^{-2} \, \text{kei}_1 \, \zeta) \right.$$
$$\left. + C_2 \, (-\zeta^{-1} \, \text{ker}_1' \, \zeta + \zeta^{-2} \, \text{ker}_1 \, \zeta) \right] \tag{B-14}$$

$$N_{\theta\phi 1} = \frac{Et \, \Psi \, \phi}{a \, \sin \phi} \left[C_1 \, (\zeta^{-1} \, \text{kei}_1' \, \zeta - \zeta^{-2} \, \text{kei}_1 \, \zeta) \right.$$
$$\left. + C_2 \, (-\zeta^{-1} \, \text{ker}_1' \, \zeta + \zeta^{-2} \, \text{ker}_1 \, \zeta) \right] \tag{B-15}$$

$$M_{\theta 1} = \frac{H\Psi}{a} \left[-C_1 \left\{ \mu \, \text{kei}_1 \, \zeta - (1 - \mu)(\zeta^{-1} \, \text{ker}_1' \, \zeta - \zeta^{-2} \, \text{ker}_1 \, \zeta) \right\} \right.$$
$$\left. + C_2 \left\{ \mu \, \text{ker}_1 \, \zeta + (1 - \mu)(\zeta^{-1} \, \text{kei}_1' \, \zeta - \zeta^{-2} \, \text{kei}_1 \, \zeta) \right\} \right] \tag{B-16}$$

$$M_{\phi 1} = \frac{H\Psi}{a} \left[-C_1 \left\{ \text{kei}_1 \, \zeta + (1 - \mu)(\zeta^{-1} \, \text{ker}_1' \, \zeta - \zeta^{-2} \, \text{ker}_1 \, \zeta) \right\} \right.$$
$$\left. + C_2 \left\{ \text{ker}_1 \, \zeta - (1 - \mu)(\zeta^{-1} \, \text{kei}_1' \, \zeta - \zeta^{-2} \, \text{kei}_1 \, \zeta) \right\} \right] \tag{B-17}$$

$$M_{\theta\phi 1} = \frac{(1-\mu)H\phi\Psi}{a \, \sin \phi} \left[C_1 \, (-\zeta^{-1} \, \text{ker}_1' \, \zeta + \zeta^{-2} \, \text{ker}_1 \, \zeta) \right.$$
$$\left. + C_2 (-\zeta^{-1} \, \text{kei}_1' \, \zeta + \zeta^{-2} \, \text{kei}_1 \, \zeta) \right] \tag{B-18}$$

$$Q_{\phi 1} = \frac{Et\Psi}{a} \zeta^{-1} \left[-C_1 \, \text{kei}_1' \, \zeta + C_2 \, \text{ker}_1' \, \zeta \right] \, . \tag{B-19}$$

The above solution decreases exponentialy with increasing ζ where

$$\zeta = \frac{a}{\ell} \phi$$

$$\Psi = \sqrt{\frac{\phi}{\sin \phi}} \quad .$$

The Bessel functions kei1 and ker1 and their derivatives are related to the Bessel functions kei and ker by:

$$\text{ker}_1 \, \zeta = \frac{1}{\sqrt{2}} (\text{ker}' \, \zeta - \text{kei}' \, \zeta)$$

$$\text{kei}_1 \, \zeta = \frac{1}{\sqrt{2}} (\text{ker}' \, \zeta + \text{kei}' \, \zeta)$$

$$\text{ker}_1' \ \zeta = \frac{1}{\sqrt{2}} \ (-\text{kei} \ \zeta - \zeta^{-1} \ \text{ker}' \ \zeta - \text{ker} \ \zeta + \zeta^{-1} \ \text{kei}' \ \zeta)$$

$$\text{kei}_1' \ \zeta = \frac{1}{\sqrt{2}} \ (-\text{kei} \ \zeta - \zeta^{-1} \ \text{ker}' \ \zeta + \text{ker} \ \zeta - \zeta^{-1} \ \text{kei}' \ \zeta).$$

Values of the functions kei, ker, kei', and ker' tabulated in Reference (8) were used for calculations.

The boundary conditions at ϕ_0 (see Figure 7) require that the hoop strain be zero and that the rotation of the boundary be equal to that of a rigid ring. Thus:

$$\text{B. C. (1)} \ \ \epsilon_\theta = 0 \rightarrow N_{\theta 1} = \mu N_{\phi 1} \ \text{at} \ \phi_0$$

$$\text{B. C. (2)} \ \ w_1 \cot \phi - \frac{\partial w_1}{\partial \phi} = 0 \ \text{at} \ \phi_0 \ .$$

Introducing Equations (B-5), (B-13), and (B-14) into the equation for

Boundary Condition (1), and Equations (B-9), (B-12), $\dfrac{\partial (B-9)}{\partial \phi}$, and $\dfrac{\partial (B-12)}{\partial \phi}$ into the equation for Boundary Condition (2); and solving simultaneously for C_1 and C_2 yields for the parameters:

$$D = 117 \ \text{lb-in.}$$

$$\ell = 0.386 \ \text{in.}$$

$$H = 7650 \ \text{lb}$$

$$C_1 = 515 \ \chi$$

$$C_2 = -519 \ \chi,$$

where

$$\chi = \frac{4(1 + \mu) F_X}{Et \ \pi} = 3.39 \times 10^{-6} \ F_X \ .$$

Substituting these back into the equations for normal deflection w_1, membrane forces $N_{\theta 1}$ and $N_{\phi 1}$, and bending moments M_θ and M_ϕ yields:

$$w_1 = -0.233 \ \chi$$

$$N_{\phi 1} = \frac{1}{\mu} N_{\theta 1} = 0.597 \ \frac{Et \ \chi}{a}$$

$$M_{\phi 1} = -0.240 \ \frac{H \ \chi}{a}$$

$$M_{\phi 1} = -0.592 \ \frac{H \ \chi}{a} \ .$$

Thus

Deflection, $w = -0.790 \times 10^{-6} \, F_X$

Stress, $\sigma_\phi = \mp \dfrac{6 M_\phi}{t^2} + \dfrac{N_\phi}{t} = \pm 3.78 \, F_X + 2.08 \, F_X$

Stress, $\sigma_\theta = \mp \dfrac{6 M_\theta}{t^2} + \dfrac{N_\theta}{t} = \pm 1.53 \, F_X + 0.69 \, F_X$.

Antimetric Bending

The calculation procedure for the antimetric bending moment M (see Figure 7) was exactly like that for the antimetric force F_X above, except that the balance of the moment M by the membrane theory gave:

$$N_{\phi 1} = -N_{\theta 1} = \frac{M}{\pi b^2} \csc \phi \qquad \text{(B-20)}$$

$$N_{\theta \phi 1} = \frac{M}{\pi b^2} \cot \phi \quad . \qquad \text{(B-21)}$$

The membrane deflections again found from an integral solution using the stress-strain relations resulted in:

$$u_1 = -\frac{\kappa}{2} \left[2 \log 2 \csc \phi + \cos \phi \log \tan \frac{\phi}{2} - \frac{1}{2} \right] \qquad \text{(B-22)}$$

$$v_1 = -\frac{\kappa}{2} \left[\log \tan \frac{\phi}{2} + \frac{1}{2} \cos \phi \right] \qquad \text{(B-23)}$$

$$w_1 = \frac{\kappa}{4} \left[3 \csc \phi - \sin \phi \right] \quad . \qquad \text{(B-24)}$$

With the same boundary conditions as above, the general solution gave:

$$C_1 = -1003 \, \kappa$$

$$C_2 = -346 \, \kappa,$$

where

$$\kappa = \frac{4 \, a \, (1 + \mu) \, M}{Et \, \pi \, b^2}$$

$$= 3.39 \times 10^{-6} \, M \quad .$$

Substituting these back into the equations for normal deflection w_1, membrane forces $N_{\theta 1}$ and $N_{\phi 1}$ and bending moments $M_{\theta 1}$ and $M_{\phi 1}$ yielded:

$$w_1 = 2.735 \, \kappa$$

$$N_{\phi 1} = \frac{1}{\mu} N_{\theta 1} = 0.490 \frac{Et \, \kappa}{a}$$

$$M_{\theta 1} = -0.380 \frac{H \kappa}{a}$$

$$M_{\phi 1} = -1.236 \frac{H \kappa}{a} \quad .$$

Thus

Deflection, $w = 9.27 \times 10^{-6}$ M

Stress, $\sigma_\phi = \overline{+} \frac{6 M_\phi}{t^2} + \frac{N_\phi}{t} = \pm 7.90$ M $+ 1.71$ M

Stress, $\sigma_\theta = \overline{+} \frac{6 M_\theta}{t^2} + \frac{N_\theta}{t} = \pm 2.43$ M $+ 0.56$ M

Natural Frequency

The natural frequency of the frame with attached covers was estimated by the inextensional theory first used by Lord Rayleigh[9] in 1881. The frame was assumed to be a complete spherical shell with two trunnion openings at $\phi_1 = 20$ and $\phi_2 = 160$ as shown in Figure B-2.
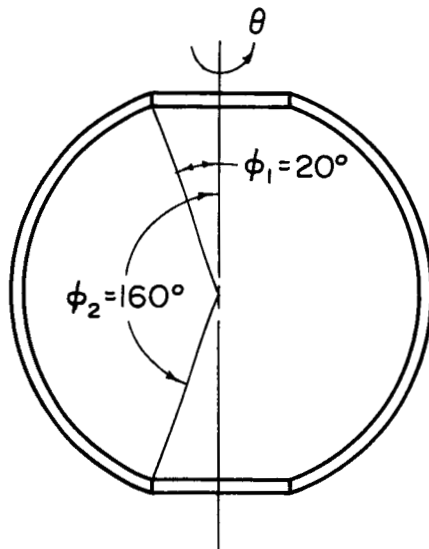
FIGURE B-2. ASSUMED SHELL SHAPE OF FRAME FOR
CALCULATION OF NATURAL FREQUENCY

It is assumed that the displacements are harmonic functions of the form:

$$u = u_n (\phi) \sin n\theta, \quad v = v_n (\phi) \cos n\theta, \quad w = w_n (\phi) \cos n\theta; \qquad \text{(B-25)}$$

u_n, v_n, and w_n for inextensional deformations are given by Flügge [Reference (5), page 90].

These are:

$$u_n = \sin \phi \left[A \tan^n \frac{\phi}{2} - B \cot^n \frac{\phi}{2} \right] \tag{B-26}$$

$$v_n = \sin \phi \left[A \tan^n \frac{\phi}{2} + B \cot^n \frac{\phi}{2} \right] \tag{B-27}$$

$$w_n = -A (n + \cos \phi) \tan^n \frac{\phi}{2} + B (n - \cos \phi) \cot^n \frac{\phi}{2} \quad . \tag{B-28}$$

(For n = 0, 1 these equations represent rigid-body motions. Thus the theory is good only for $n \geqq 2$.) The change in curvature and twist also given by Flügge [Reference (5), page 387] are:

$$\kappa_\phi = -\kappa_\theta = -\frac{n (n^2 - 1)}{a^2 \sin^2 \phi} \left(A \tan^n \frac{\phi}{2} - B \cot^n \frac{\phi}{2} \right) \cos n \theta \tag{B-29}$$

$$\kappa_{\theta\phi} = \frac{n (n^2 - 1)}{a^2 \sin^2 \phi} \left(A \tan^n \frac{\phi}{2} + B \cot^n \frac{\phi}{2} \right) \sin n \theta \quad . \tag{B-30}$$

The potential strain energy of bending from Novozhilov [Reference (10), page 47] is:

$$V = \frac{D}{2} \int_{\phi_1}^{\phi_2} \int_0^{2\pi} \left[(\kappa_\phi + \kappa_\theta)^2 - 2 (1 - \mu) (\kappa_\theta \kappa_\phi - \kappa_{\theta\phi}^2) \right] a^2 \sin \phi \, d\theta \, d\phi \quad . \tag{B-31}$$

The kinetic energy due to vibration is:

$$T = \frac{1}{2} \int_{\phi_1}^{\phi_2} \int_0^{2\pi} \frac{\rho t \, a^2}{g} (\dot{u}^2 + \dot{v}^2 + \dot{w}^2) \sin \phi \, d\theta \, d\phi \quad , \tag{B-32}$$

where

$$\dot{u} = \frac{du}{dt} \quad .$$

Lagrange's equations of motion state that

$$\frac{d}{dt} \left(\frac{\partial T}{\partial \dot{A}} \right) + \frac{\partial V}{\partial A} = 0 \tag{B-33}$$

$$\frac{d}{dt} \left(\frac{\partial T}{\partial \dot{B}} \right) + \frac{\partial V}{\partial B} = 0 \quad .$$

In general the vibration will be coupled as indicated by Equations (B-33). To find the lowest normal mode corresponding to the A component, let B = 0 and let

$$A = A' \cos (\omega t + \gamma) \quad . \tag{B-34}$$

The lowest frequency occurs for n = 2 as shown by Naghdi and Kalnins and others. Letting n = 2, and substituting Equations (B-26) to (B-30) into (B-31) and (B-32), and then further substituting the resulting equations into (B-33) results in:

$$\omega = 498\, \frac{t}{a^2}\, \sqrt{\frac{E\,(1-\mu)}{\rho}}, \text{ radians/sec.} \tag{B-35}$$

The frequency f is

$$f = \frac{\omega}{2\pi} = 79.3\, \frac{t}{a^2}\, \sqrt{\frac{E\,(1-\mu)}{\rho}}, \text{ cycles/sec.} \tag{B-36}$$

APPENDIX C

STRESSES AND DEFLECTIONS IN PROPOSED DESIGN
FOR AN 8-G LINEAR ACCELERATION

APPENDIX C

STRESSES AND DEFLECTIONS IN PROPOSED DESIGN FOR AN 8-G LINEAR ACCELERATION

Calculation of the Maximum Primary Bending Stress and Associated Orientation of Acceleration

The equations shown below may be used in conjunction with the stress curves included in this appendix.

The nomenclature used in these equations is as follows:

σ_X = stress due to acceleration in the X-direction

σ_Y = stress due to acceleration in the Y-direction

σ_Z = stress due to acceleration in the Z-direction

σ_{ZY} = stress due to acceleration in the ZY plane (plane of middle gimbal)

σ_{ZX} = stress due to acceleration in the ZX plane (plane of outer and redundant gimbal)

θ_M = orientation of acceleration in plane of gimbal which produces the maximum stress at the point under consideration (measured from + Z axis, $-90° \leq \theta_M \leq + 90°$)

Ψ_M = orientation of acceleration from plane of gimbal which produces the maximum stress at the point under consideration (measured from plane of gimbal, $-90° \leq \Psi_M \leq + 90°$).

For the middle gimbal (Figures C-2, C-3 and C-4):

$$\theta_M = \tan^{-1}\left(\frac{\sigma_Y}{\sigma_Z}\right) \tag{C-1}$$

$$\sigma_{ZY} = \sigma_Z \cos \theta_M + \sigma_Y \sin \theta_M \tag{C-2}$$

$$\Psi_M = \tan^{-1}\left(\frac{\sigma_X}{\sigma_{ZY}}\right) \tag{C-3}$$

$$\sigma_{MAX} = \sigma_{ZY} \cos \Psi_M + \sigma_X \sin \Psi_M \tag{C-4}$$

For the outer gimbal (Figures C-6, C-7 and C-8):

$$\theta_M = \tan^{-1}\left(\frac{\sigma_X}{\sigma_Z}\right) \tag{C-5}$$

$$\sigma_{ZX} = \sigma_Z \cos \theta_M + \sigma_X \sin \theta_M \tag{C-6}$$

$$\Psi_M = \tan^{-1}\left(\frac{\sigma_Y}{\sigma_{ZX}}\right) \tag{C-7}$$

$$\sigma_{MAX} = \sigma_{ZX} \cos \Psi_M + \sigma_Y \sin \Psi_M \tag{C-8}$$

For the redundant gimbal (Figures C-10, C-11 and C-12):

$$\theta_M = \tan^{-1}\left(\frac{\sigma_X}{\sigma_Z}\right) \tag{C-9}$$

$$\sigma_{ZX} = \sigma_Z \cos \theta_M + \sigma_X \sin \theta_M \tag{C-10}$$

$$\Psi_M = \tan^{-1}\left(\frac{\sigma_Y}{\sigma_{ZX}}\right) \tag{C-11}$$

$$\sigma_{MAX} = \sigma_{ZX} \cos \Psi_M + \sigma_Y \sin \Psi_M \tag{C-12}$$
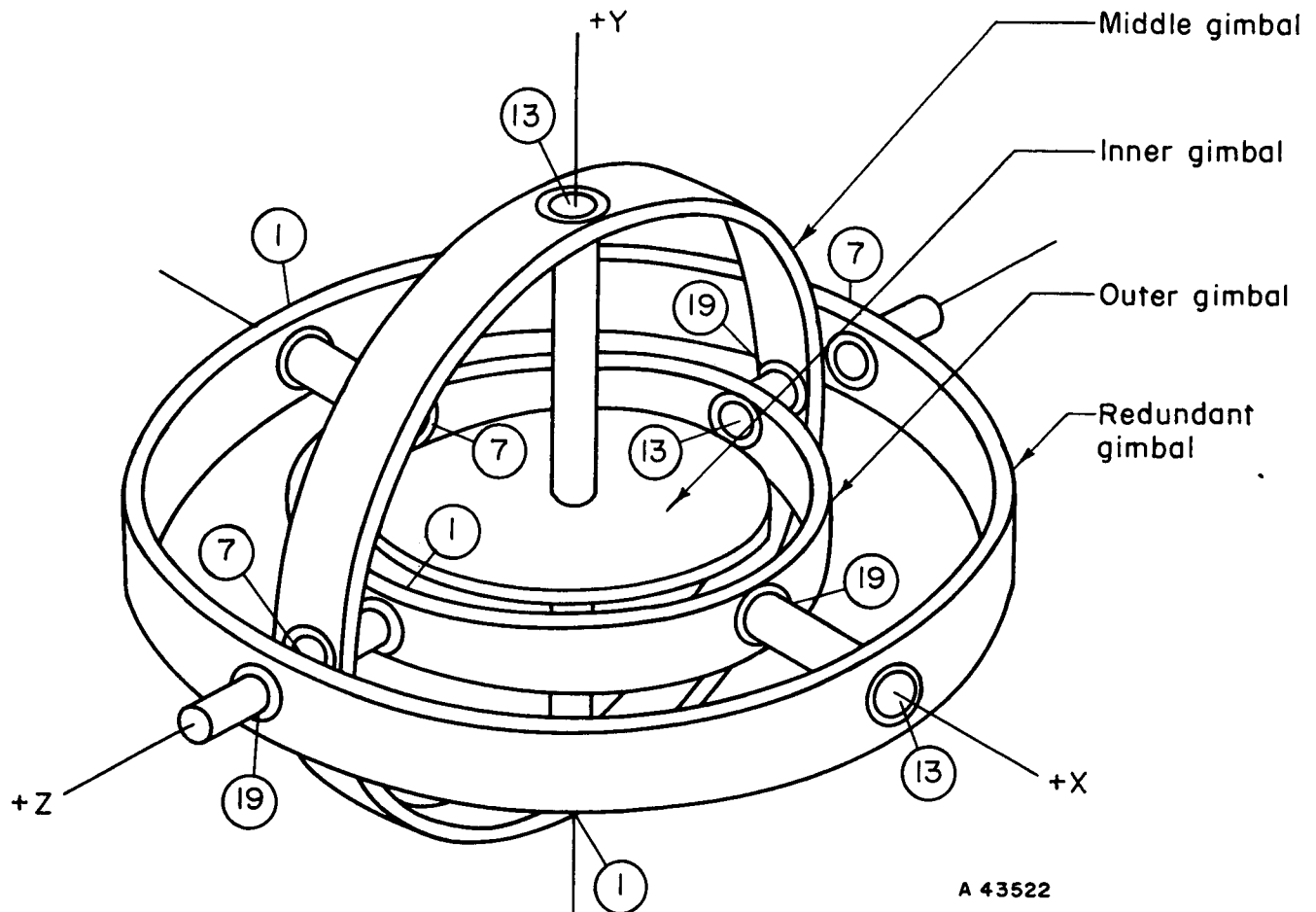
FIGURE C-1. PLATFORM SCHEMATIC SHOWING SUPPORT LOCATIONS
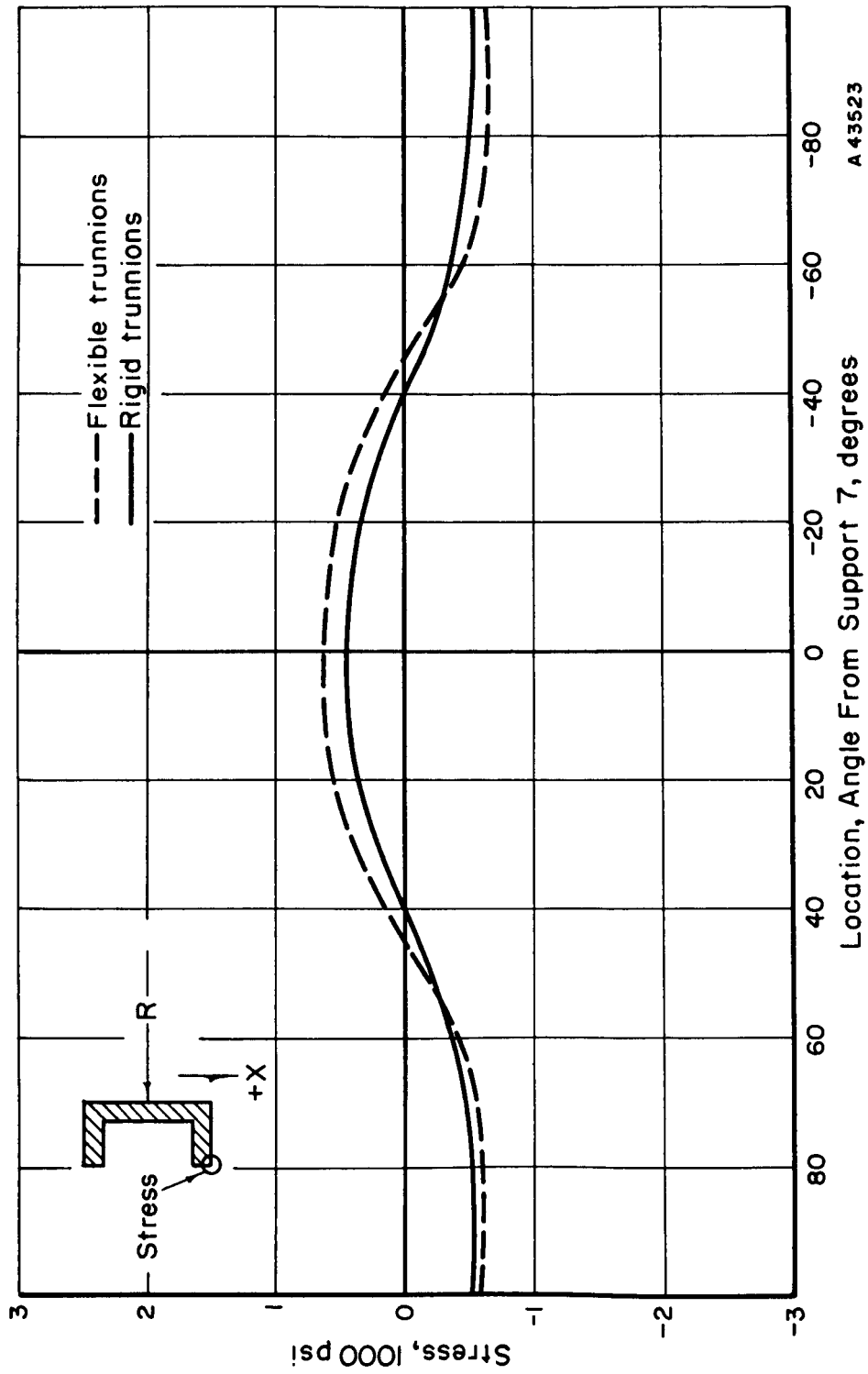
FIGURE C-2. STRESS IN MIDDLE GIMBAL FOR AN 8-g ACCELERATION IN THE + x - DIRECTION

A43523
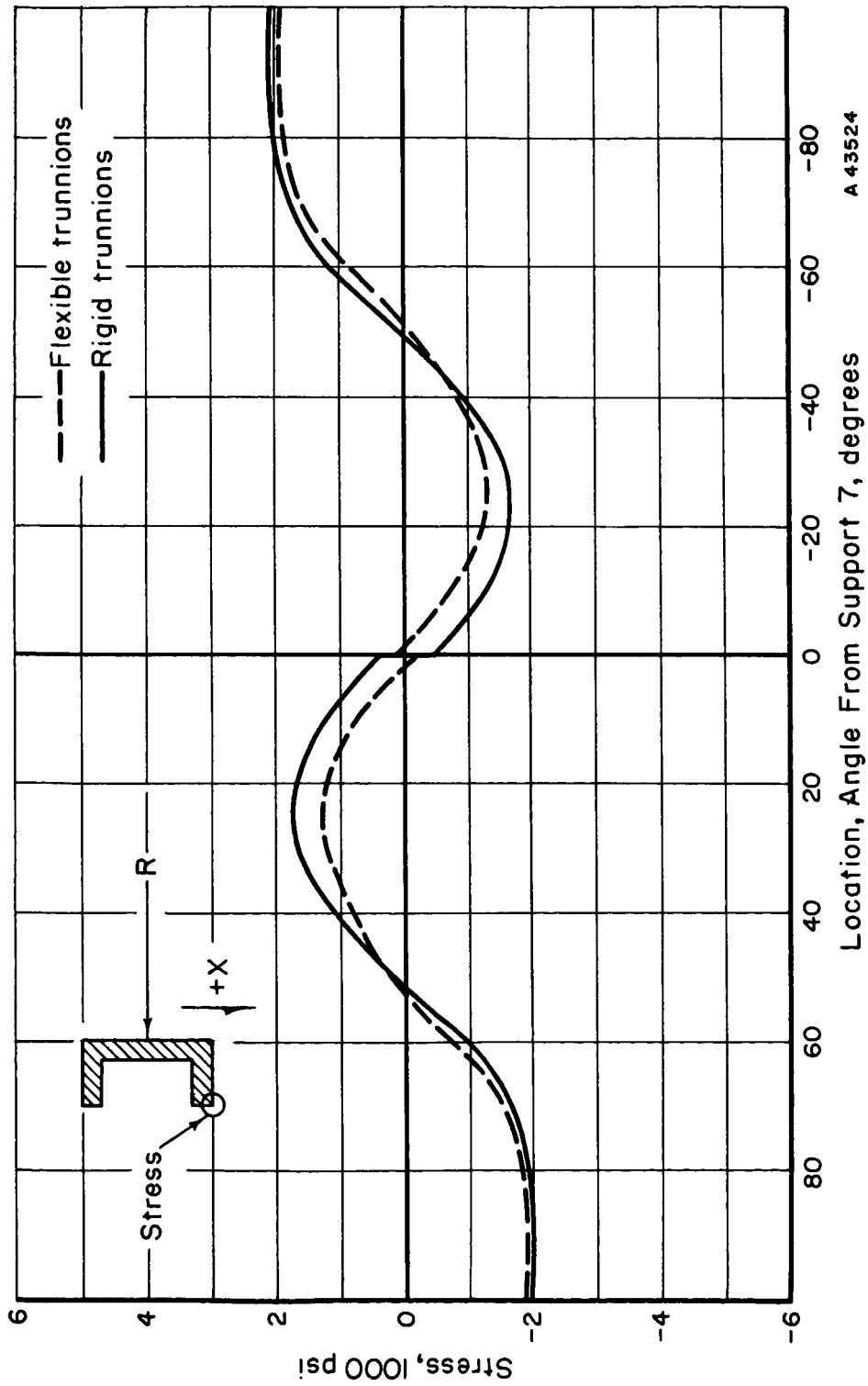
FIGURE C-3. STRESS IN MIDDLE GIMBAL FOR AN 8-g ACCELERATION IN THE + Y DIRECTION
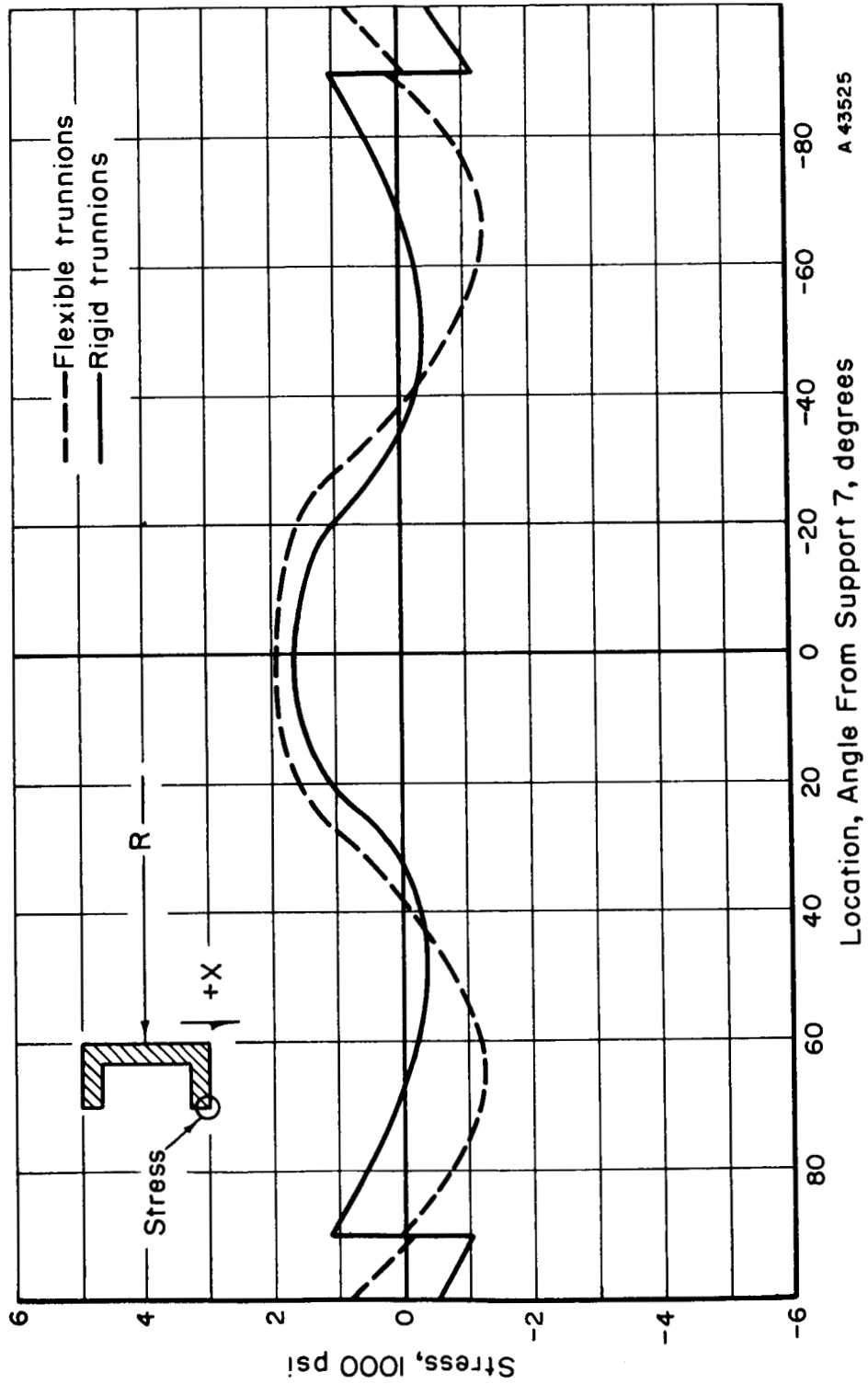
FIGURE C-4. STRESS IN MIDDLE GIMBAL FOR AN 8-g ACCELERATION IN THE + Z DIRECTION
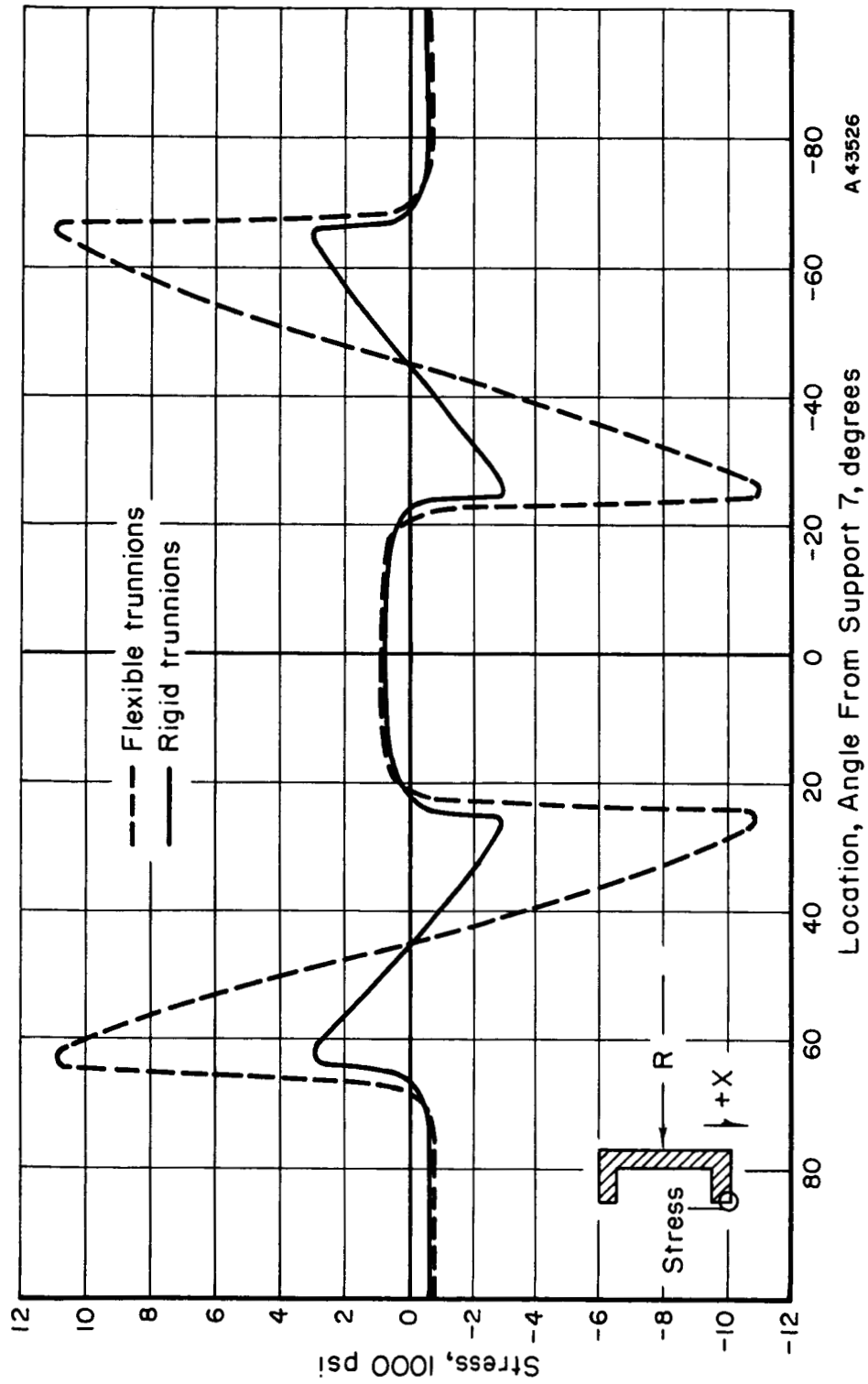
A 43525

FIGURE C-5. SECONDARY FLANGE BENDING STRESS IN MIDDLE GIMBAL FOR AN 8-g ACCELERATION
IN THE + X DIRECTION
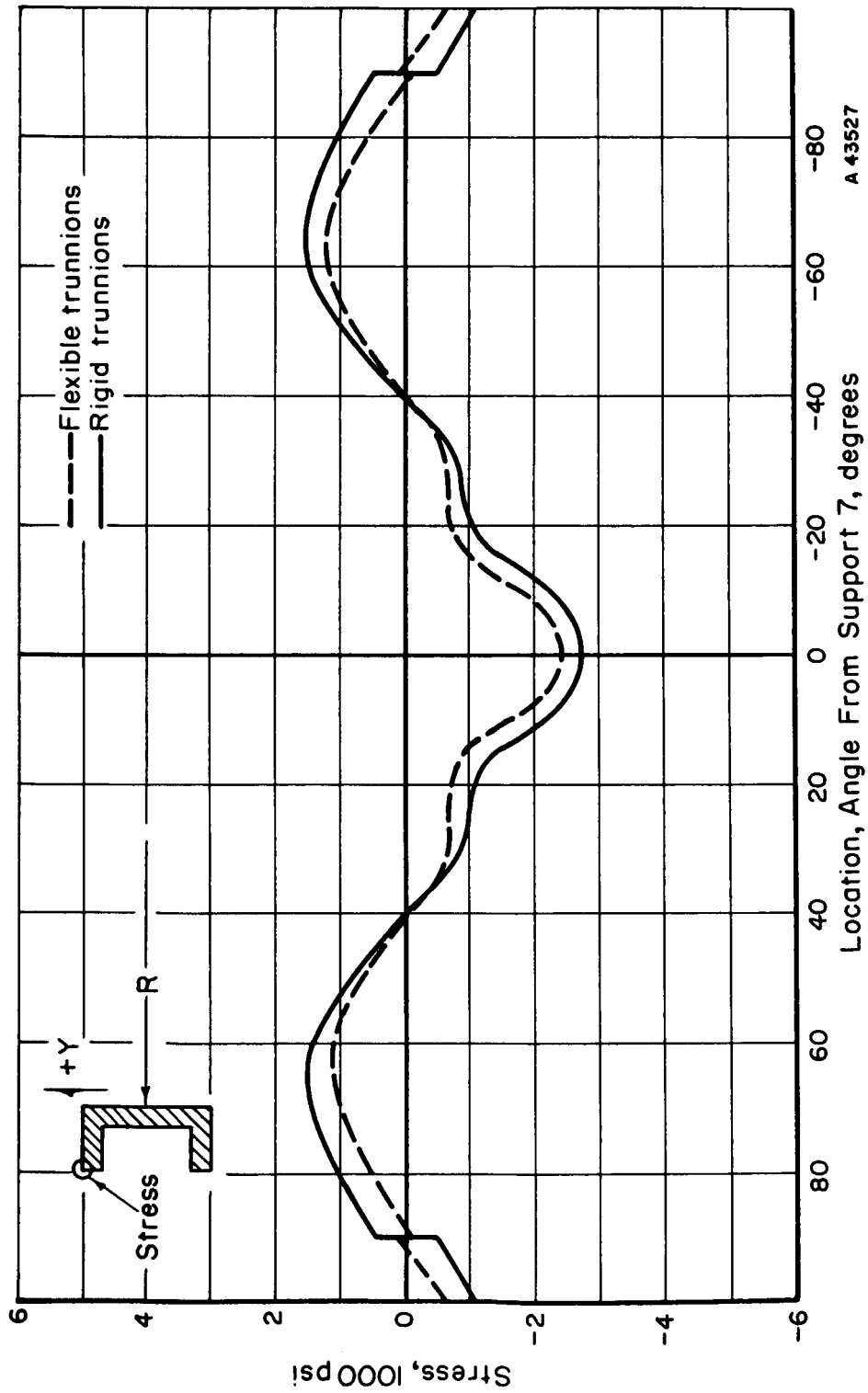
FIGURE C-6. STRESS IN OUTER GIMBAL FOR AN 8-g ACCELERATION IN THE + X DIRECTION
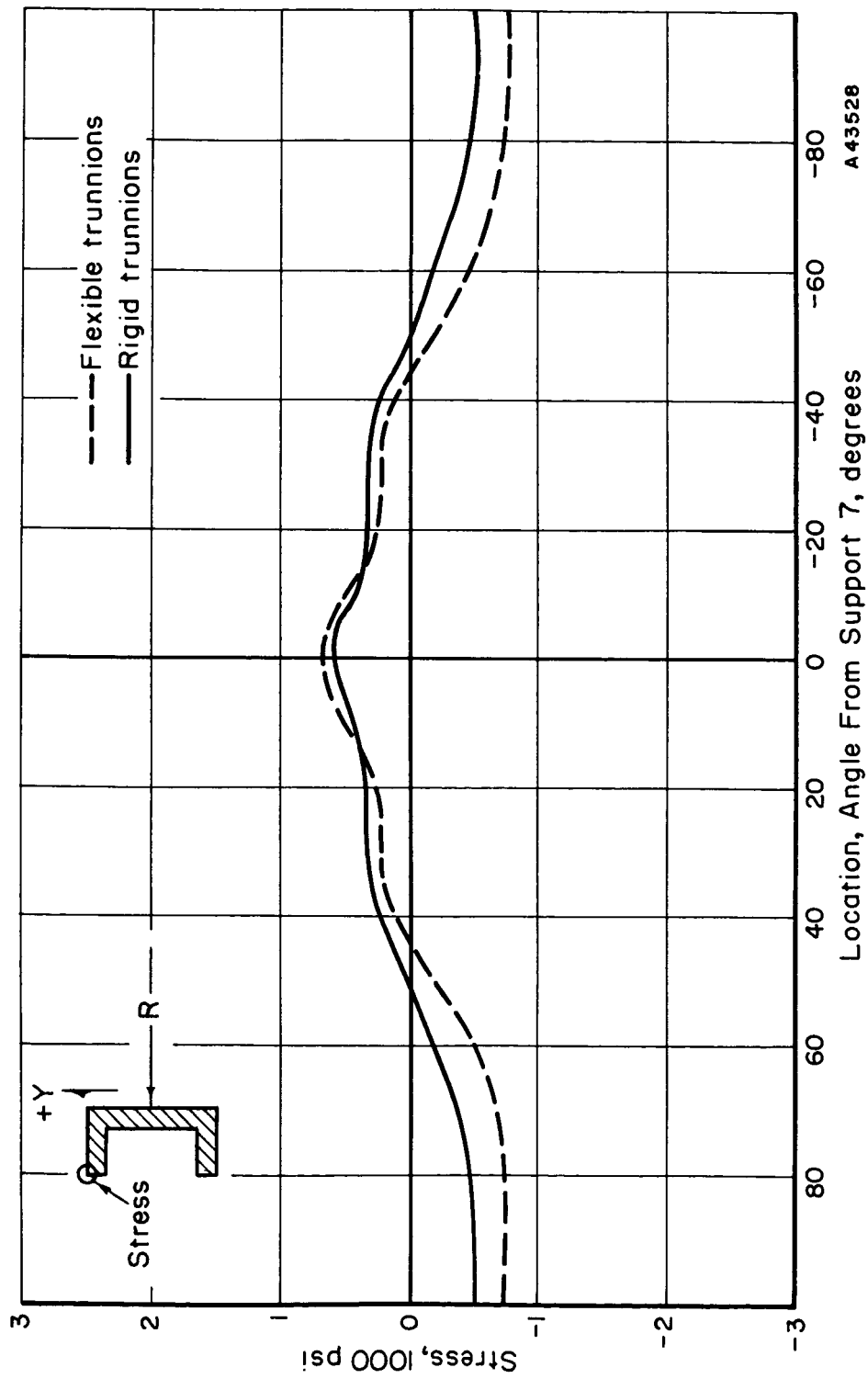
FIGURE C-7. STRESS IN OUTER GIMBAL FOR AN 8-g ACCELERATION IN THE + Y DIRECTION
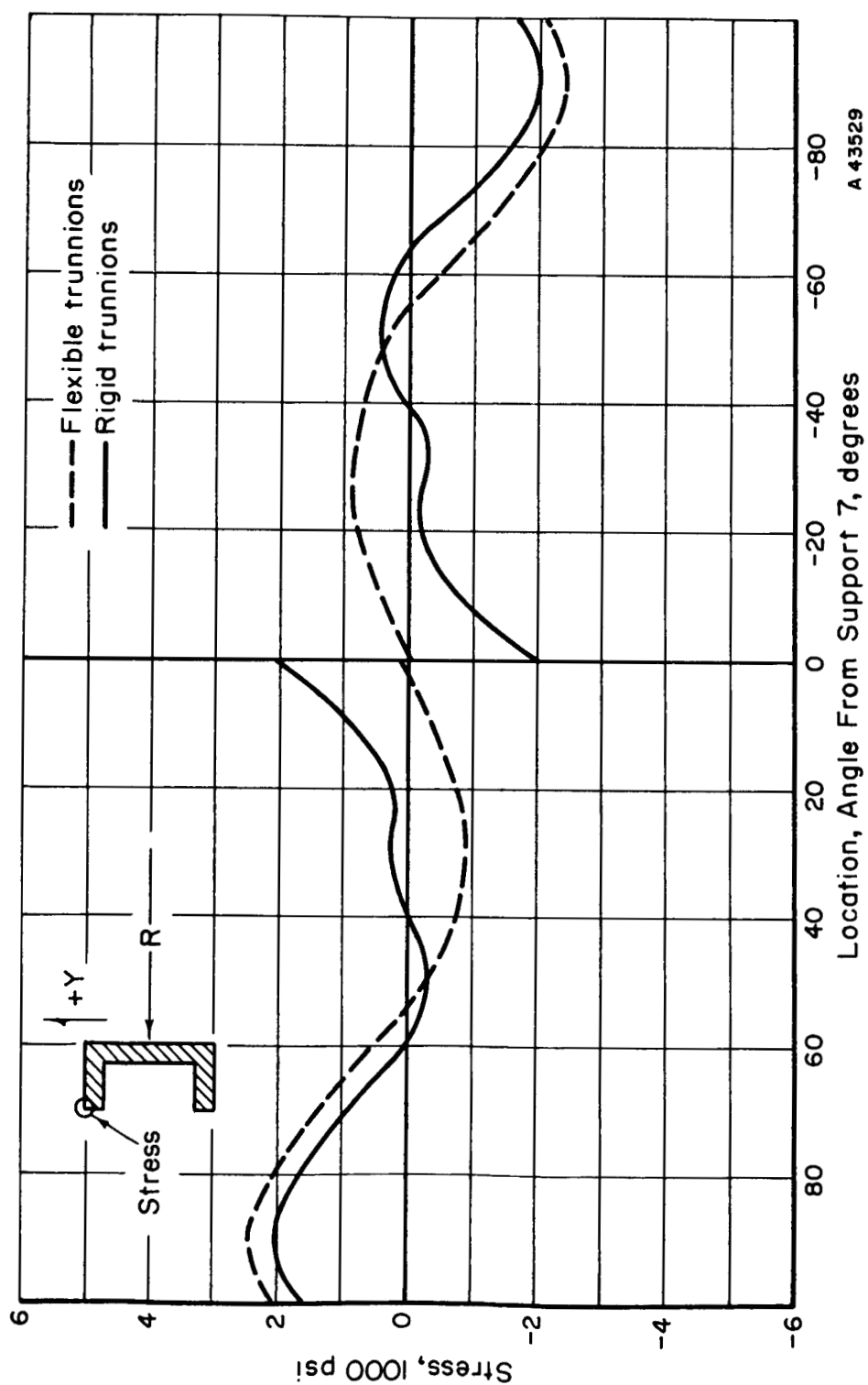
FIGURE C-8. STRESS IN OUTER GIMBAL FOR AN 8-g ACCELERATION IN THE + Z DIRECTION
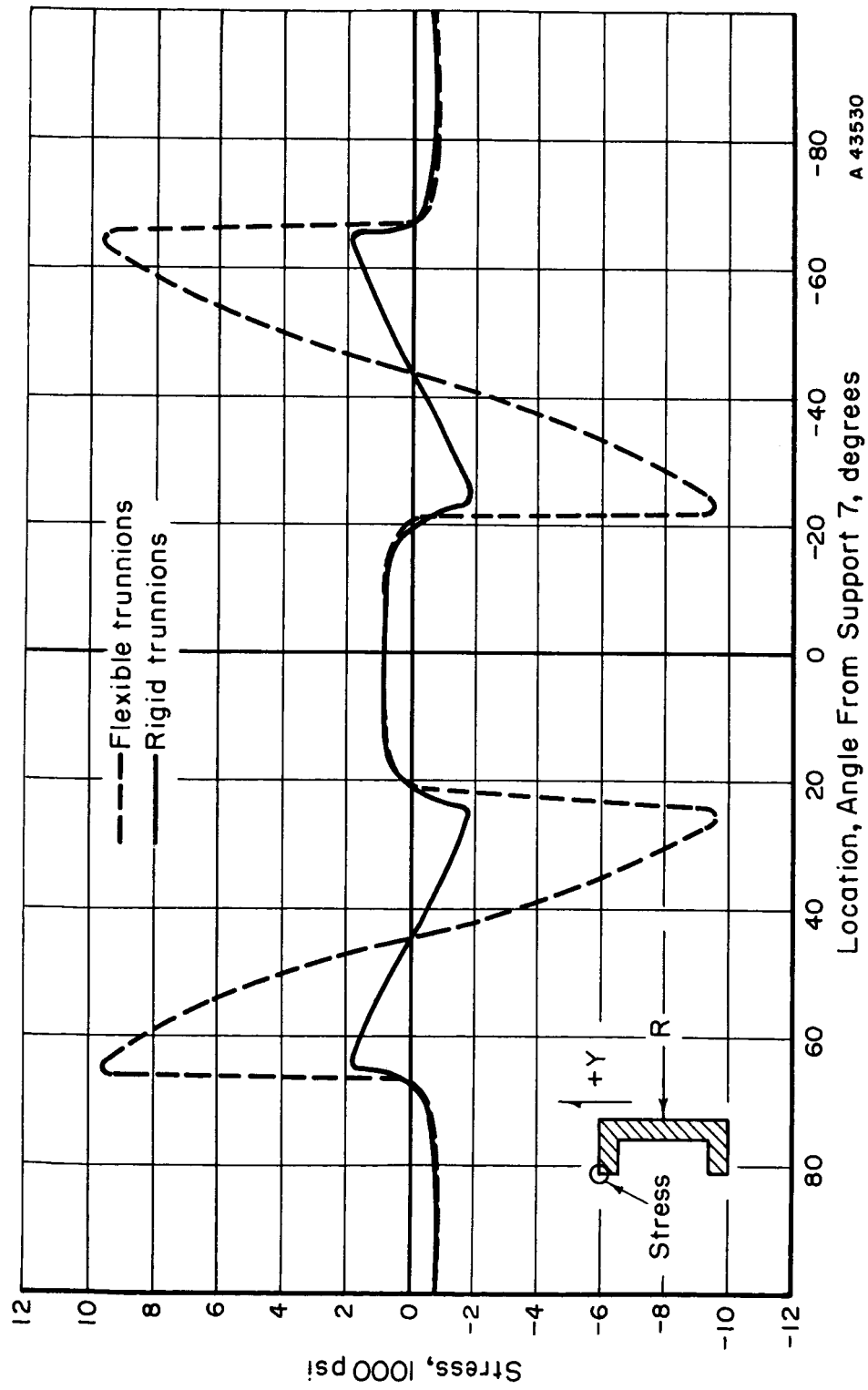
FIGURE C-9. SECONDARY FLANGE BENDING STRESS IN OUTER GIMBAL FOR AN 8-g ACCELERATION IN THE + Y DIRECTION
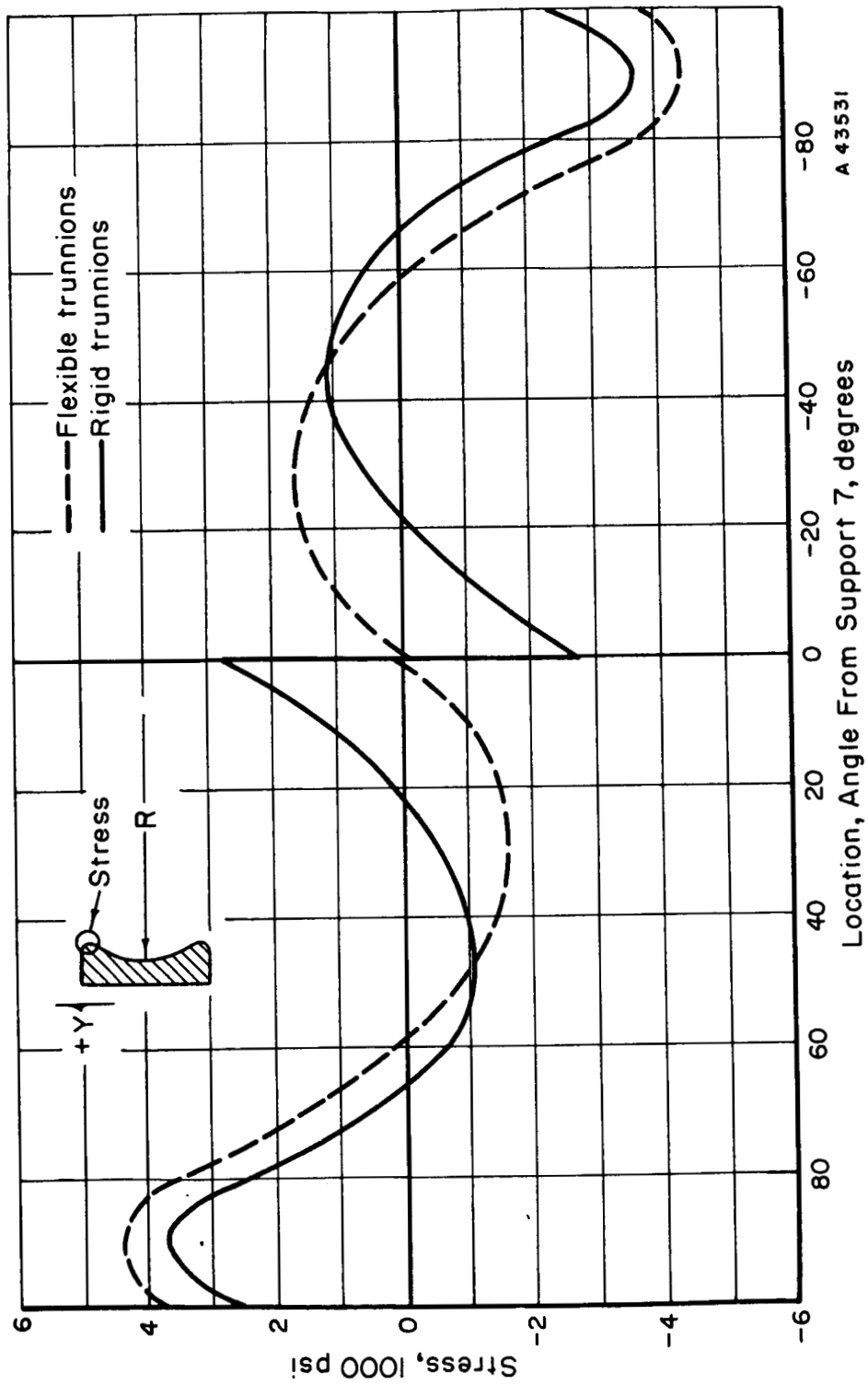
FIGURE C-10. STRESS IN REDUNDANT GIMBAL FOR AN 8-g ACCELERATION IN THE + X DIRECTION
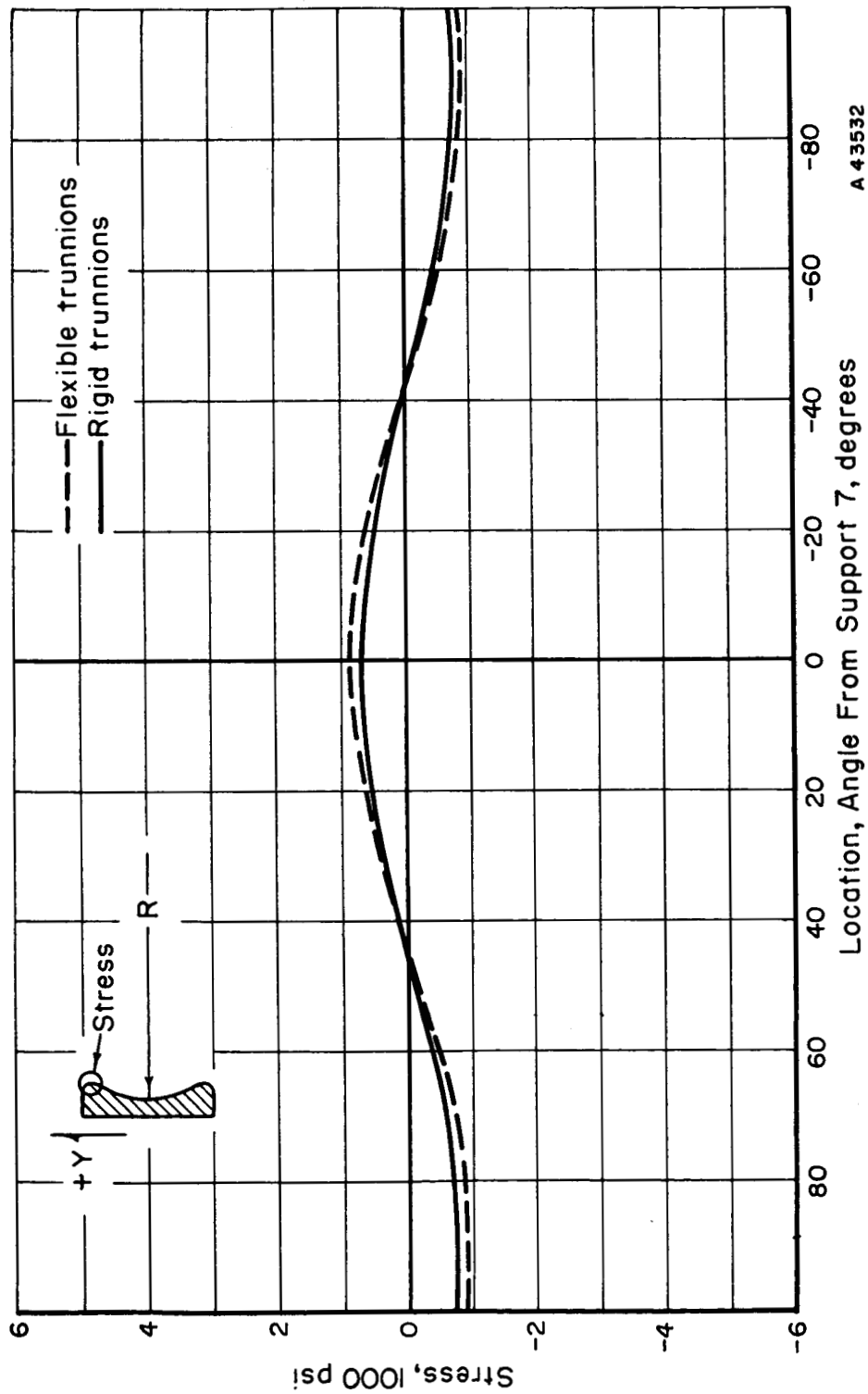
FIGURE C-11. STRESS IN REDUNDANT GIMBAL FOR AN 8-g ACCELERATION IN THE + Y DIRECTION
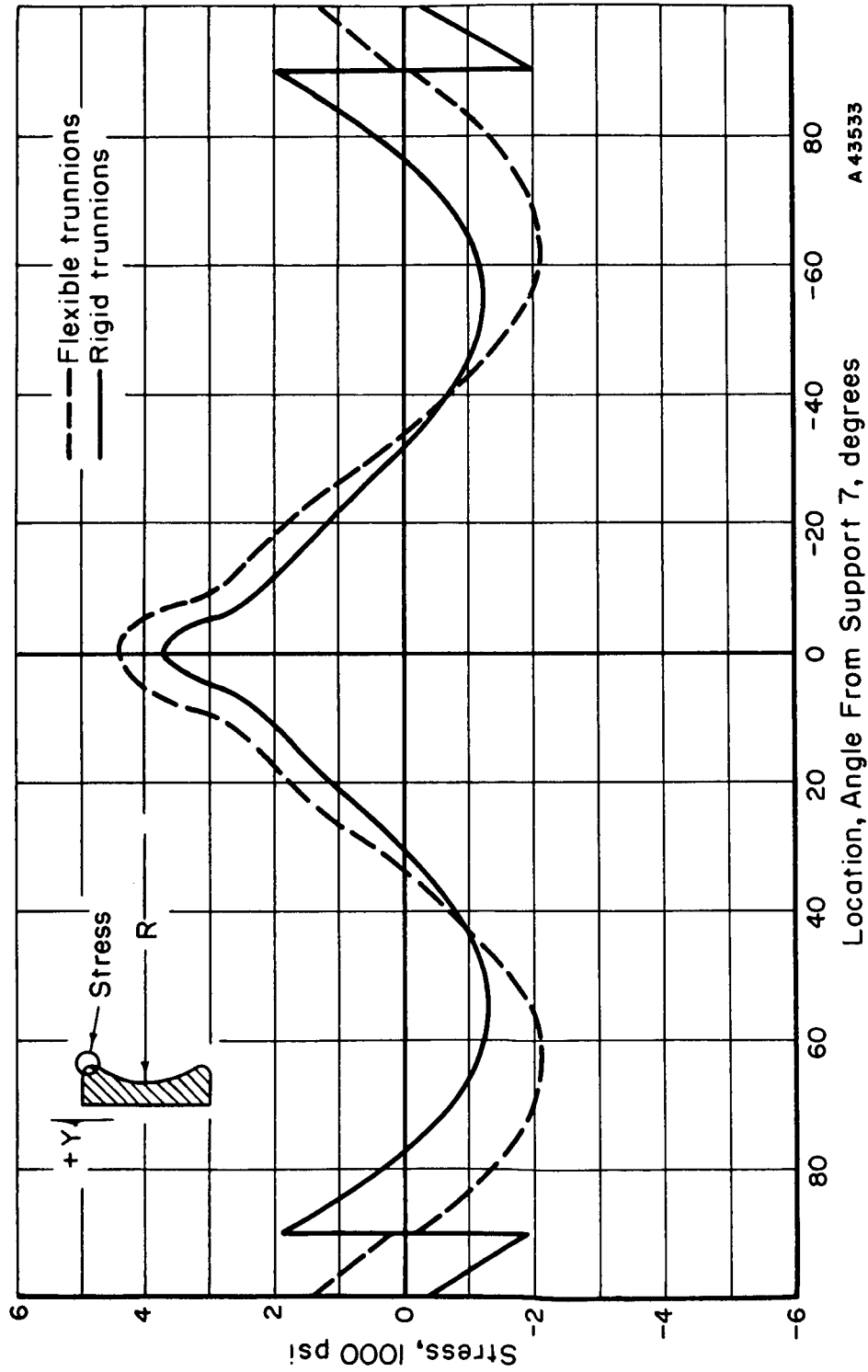
FIGURE C-12. STRESS IN REDUNDANT GIMBAL FOR AN 8-g ACCELERATION IN THE + Z DIRECTION

TABLE C-1. ABSOLUTE DISPLACEMENTS[a] FOR AN 8-G
LINEAR ACCELERATION IN +X DIRECTION
WITH FLEXIBLE TRUNNIONS

| | Displacement, 10^{-6} inches | | | | | | | | |
| | Middle Gimbal | | | Outer Gimbal | | | Redundant Gimbal | | |
Node	X	Y	Z	X	Y	Z	X	Y	Z
1	-3082	0	0	-1614	0	0	-1415	0	0
2	-3068	0	0	-1612	0	+112	-636	0	-3
3	-2747	0	0	-1612	0	+118	-173	0	+323
4	-2350	0	0	-1574	0	+81	+75	0	+597
5	-1950	0	0	-1511	0	+42	+69	0	+578
6	-1628	0	0	-1474	0	-1	-3	0	+428
7	-1614	0	0	-1415	0	0	0	0	0
8	-1628	0	0	-1474	0	+1	-3	0	-428
9	-1950	0	0	-1511	0	-42	+69	0	-578
10	-2350	0	0	-1574	0	-81	+75	0	-597
11	-2747	0	0	-1612	0	-118	-173	0	-323
12	-3068	0	0	-1612	0	-112	-636	0	+3
13	-3082	0	0	-1614	0	0	-1415	0	0
14	-3068	0	0	-1612	0	+112	-636	0	-3
15	-2747	0	0	-1612	0	+118	-173	0	+323
16	-2350	0	0	-1574	0	+81	+75	0	+597
17	-1950	0	0	-1511	0	+42	+69	0	+578
18	-1628	0	0	-1474	0	-1	-3	0	+428
19	-1614	0	0	-1415	0	0	0	0	0
20	-1628	0	0	-1474	0	+1	-3	0	-428
21	-1950	0	0	-1511	0	-42	+69	0	-578
22	-2350	0	0	-1574	0	-81	+75	0	-597
23	-2747	0	0	-1612	0	-118	-173	0	-323
24	-3068	0	0	-1612	0	-112	-635	0	+3

(a) Displacement of neutral axis.

TABLE C-2. ABSOLUTE DISPLACEMENTS[a] FOR AN 8-G
LINEAR ACCELERATION IN +Y DIRECTION
WITH FLEXIBLE TRUNNIONS

	Displacements, 10^{-6} inches								
	Middle Gimbal			Outer Gimbal			Redundant Gimbal		
Node	X	Y	Z	X	Y	Z	X	Y	Z
1	0	-5325	0	0	-5039	0	0	-4171	0
2	0	-5251	0	0	-5024	0	0	-4066	0
3	0	-5171	-39	0	-4856	0	0	-2955	0
4	0	-5086	-107	0	-4642	0	0	-1714	0
5	0	-5039	-158	0	-4339	0	0	-599	0
6	0	-5042	-146	0	-4183	0	0	-199	0
7	0	-5039	0	0	-4171	0	0	0	0
8	0	-5042	+146	0	-4183	C	0	-199	0
9	0	-5039	+158	0	-4339	0	0	-599	0
10	0	-5086	+107	0	-4642	0	0	-1714	0
11	0	-5171	+39	0	-4856	0	0	-2955	0
12	0	-5251	0	0	-5024	0	0	-4066	0
13	0	-5325	0	0	-5039	0	0	-4171	0
14	0	-5251	0	0	-5024	0	0	-4066	0
15	0	-5171	-39	0	-4856	0	0	-2955	0
16	0	-5086	-107	0	-4642	0	0	-1714	0
17	0	-5039	-158	0	-4339	0	0	-599	0
18	0	-5042	-146	0	-4183	0	0	-199	0
19	0	-5039	0	0	-4171	0	0	0	0
20	0	-5042	+146	0	-4183	0	0	-199	0
21	0	-5039	+158	0	-4339	0	0	-599	0
22	0	-5086	+107	0	-4642	0	0	-1714	0
23	0	-5171	+39	0	-4856	0	0	-2955	0
24	0	-5251	0	0	-5024	0	0	-4066	0

(a) Displacement of neutral axis.

TABLE C-3. ABSOLUTE DISPLACEMENTS[a] FOR AN 8-G
LINEAR ACCELERATION IN +Z DIRECTION
WITH FLEXIBLE TRUNNIONS

	Displacement, 10^{-6} inches								
	Middle Gimbal			Outer Gimbal			Redundant Gimbal		
Node	X	Y	Z	X	Y	Z	X	Y	Z
1	0	0	-1562	0	0	-1267	0	0	-1075
2	0	+150	-1559	+1	0	-1194	-663	0	-1069
3	0	+162	-1562	-27	0	-1133	-596	0	-1017
4	0	+111	-1516	-68	0	-1085	-294	0	-670
5	0	+42	-1429	-86	0	-1070	-62	0	-241
6	0	-1	-1345	-77	0	-1077	+1	0	-111
7	0	0	-1267	0	0	-1075	0	0	0
8	0	+1	-1345	+77	0	-1077	-1	0	-111
9	0	-42	-1429	+86	0	-1070	+62	0	-241
10	0	-111	-1516	+68	0	-1085	+294	0	-670
11	0	-162	-1562	+27	0	-1133	+596	0	-1017
12	0	-150	-1559	-1	0	-1194	+663	0	-1069
13	0	0	-1562	0	0	-1267	0	0	-1075
14	0	+150	-1559	+1	0	-1194	-663	0	-1069
15	0	+162	-1562	-27	0	-1133	-596	0	-1017
16	0	+111	-1516	-68	0	-1085	-294	0	-670
17	0	+42	-1429	-86	0	-1070	-62	0	-241
18	0	-1	-1345	-77	0	-1077	+1	0	-111
19	0	0	-1267	0	0	-1075	0	0	0
20	0	+1	-1345	+77	0	-1077	-1	0	-111
21	0	-42	-1429	+86	0	-1070	+62	0	-241
22	0	-111	-1516	+68	0	-1085	+294	0	-670
23	0	-162	-1562	+27	0	-1133	+596	0	-1017
24	0	-150	-1559	-1	0	-1194	+663	0	-1069

(a) Displacement of neutral axis.

TABLE C-4. ANGLE OF TWIST FOR AN 8-G LINEAR
ACCELERATION PERPENDICULAR TO
PLANE OF GIMBAL WITH FLEXIBLE
TRUNNIONS

| | Angle of Twist, 10^{-6} radians | | |
Node	Middle Gimbal +X Acceleration	Outer Gimbal +Y Acceleration	Redundant Gimbal +Y Acceleration
1	502	293	892
2	471	276	800
3	249	134	267
4	0	-42	-332
5	-249	-168	-733
6	-471	-230	-1060
7	-502	-281	-1122
	-Symmetrical	-Symmetrical	-Symmetrical

TABLE C-5. ANGLE OF TWIST FOR AN 8-G LINEAR
ACCELERATION PERPENDICULAR TO
PLANE OF GIMBAL WITH RIGID
TRUNNIONS

| | Angle of Twist, 10^{-6} radians | | |
Node	Middle Gimbal +X Acceleration	Outer Gimbal +Y Acceleration	Redundant Gimbal +Y Acceleration
1	0	33	24
2	50	50	88
3	50	26	22
4	7	-4	-63
5	-41	-15	-96
6	-79	-30	-108
7	-60	25	0
	-Symmetrical	-Symmetrical	-Symmetrical

TABLE C-6.   ABSOLUTE DISPLACEMENTS[a] FOR AN 8-G
LINEAR ACCELERATION IN +X DIRECTION
WITH RIGID TRUNNIONS

| | Displacements, 10^{-6} inches | | | | | | | | |
| | Middle Gimbal | | | Outer Gimbal | | | Redundant Gimbal | | |
Node	X	Y	Z	X	Y	Z	X	Y	Z
1	-1385	0	0	-1079	0	0	-855	0	0
2	-1372	0	0	-1076	0	+134	-243	0	-6
3	-1319	0	0	-1075	0	+137	+18	0	+174
4	-1241	0	0	-1031	0	+93	+72	0	+227
5	-1159	0	0	-960	0	+47	+23	0	+127
6	-1091	0	0	-918	0	0	-3	0	+69
7	-1079	0	0	-855	0	0	0	0	0
8	-1091	0	0	-918	0	0	-3	0	+69
9	-1159	0	0	-960	0	-47	+23	0	-127
10	-1241	0	0	-1031	0	-93	+72	0	-227
11	-1319	0	0	-1075	0	-137	+18	0	-174
12	-1372	0	0	-1076	0	-134	-243	0	+6
13	-1385	0	0	-1079	0	0	-855	0	0
14	-1372	0	0	-1076	0	+134	-243	0	-6
15	-1319	0	0	-1075	0	+137	+18	0	+174
16	-1241	0	0	-1031	0	+93	+72	0	+227
17	-1159	0	0	-960	0	+47	+23	0	+127
18	-1091	0	0	-918	0	0	-3	0	+69
19	-1079	0	0	-855	0	0	0	0	0
20	-1091	0	0	-918	0	0	-3	0	-69
21	-1159	0	0	-960	0	-47	+23	0	-127
22	-1241	0	0	-1031	0	-93	+72	0	-227
23	-1319	0	0	-1075	0	-137	+18	0	-174
24	-1372	0	0	-1076	0	-134	-243	0	+6

(a) Displacement of neutral axis.

TABLE C-7. ABSOLUTE DISPLACEMENTS[a] FOR AN 8-G
LINEAR ACCELERATION IN +Y DIRECTION
WITH RIGID TRUNNIONS

| | Displacements, 10^{-6} inches | | | | | | | | |
| | Middle Gimbal | | | Outer Gimbal | | | Redundant Gimbal | | |
Node	X	Y	Z	X	Y	Z	X	Y	Z
1	0	-1254	0	0	-927	0	0	-719	0
2	0	-1176	+2	0	-914	0	0	-638	0
3	0	-1085	-45	0	-873	0	0	-454	0
4	0	-985	-126	0	-821	0	0	-254	0
5	0	-928	-190	0	-774	0	0	-92	0
6	0	-930	-181	0	-731	0	0	-18	0
7	0	-927	0	0	-719	0	0	0	0
8	0	-930	+181	0	-731	0	0	-18	0
9	0	-928	+190	0	-774	0	0	-92	0
10	0	-985	+126	0	-821	0	0	-254	0
11	0	-1085	+45	0	-873	0	0	-454	0
12	0	-1176	-2	0	-914	0	0	-638	0
13	0	-1254	0	0	-927	0	0	-719	0
14	0	-1176	+2	0	-914	0	0	-638	0
15	0	-1085	-45	0	-873	0	0	-454	0
16	0	-985	-126	0	-821	0	0	-254	0
17	0	-928	-190	0	-774	0	0	-92	0
18	0	-930	-181	0	-731	0	0	-18	0
19	0	-927	0	0	-719	0	0	0	0
20	0	-930	+181	0	-731	0	0	-18	0
21	0	-928	+190	0	-774	0	0	-92	0
22	0	-985	+126	0	-821	0	0	-254	0
23	0	-1085	+45	0	-873	0	0	-454	0
24	0	-1176	-2	0	-914	0	0	-638	0

(a) Displacement of neutral axis.

TABLE C-8. ABSOLUTE DISPLACEMENTS[a] FOR AN 8-G
LINEAR ACCELERATION IN +Z DIRECTION
WITH RIGID TRUNNIONS

	Displacements, 10^{-6} inches								
	Middle Gimbal			Outer Gimbal			Redundant Gimbal		
Node	X	Y	Z	X	Y	Z	X	Y	Z
1	0	0	-963	0	0	-796	0	0	-700
2	0	+42	-961	+3	0	-739	-365	0	-694
3	0	+61	-967	-9	0	-707	-380	0	-699
4	0	+52	-954	-13	0	-697	-207	0	-497
5	0	+23	-914	-3	0	-700	-46	0	-196
6	0	-2	-861	+3	0	-702	+2	0	-95
7	0	0	-796	0	0	-700	0	0	0
8	0	+2	-861	-3	0	-702	-2	0	-95
9	0	-23	-914	+3	0	-700	+46	0	-196
10	0	-52	-954	+13	0	-697	+207	0	-497
11	0	-61	-967	+9	0	-707	+380	0	-699
12	0	-42	-961	-3	0	-739	+365	0	-694
13	0	0	-963	0	0	-796	0	0	-700
14	0	+42	-961	+3	0	-739	-365	0	-694
15	0	+61	-967	-9	0	-707	-380	0	-699
16	0	+52	-954	-13	0	-697	-207	0	-497
17	0	+23	-914	-3	0	-700	-46	0	-196
18	0	-2	-861	+3	0	-702	+2	0	-95
19	0	0	-796	0	0	-700	0	0	0
20	0	+2	-861	-3	0	-702	-2	0	-95
21	0	-23	-914	+3	0	-700	+46	0	-196
22	0	-52	-954	+13	0	-697	+207	0	-497
23	0	-61	-967	+9	0	-707	+380	0	-699
24	0	-42	-961	-3	0	-739	+365	0	-694

(a) Displacement of neutral axis.

APPENDIX D

PHYSICAL PROPERTIES OF MIDDLE, OUTER, AND REDUNDANT GIMBALS
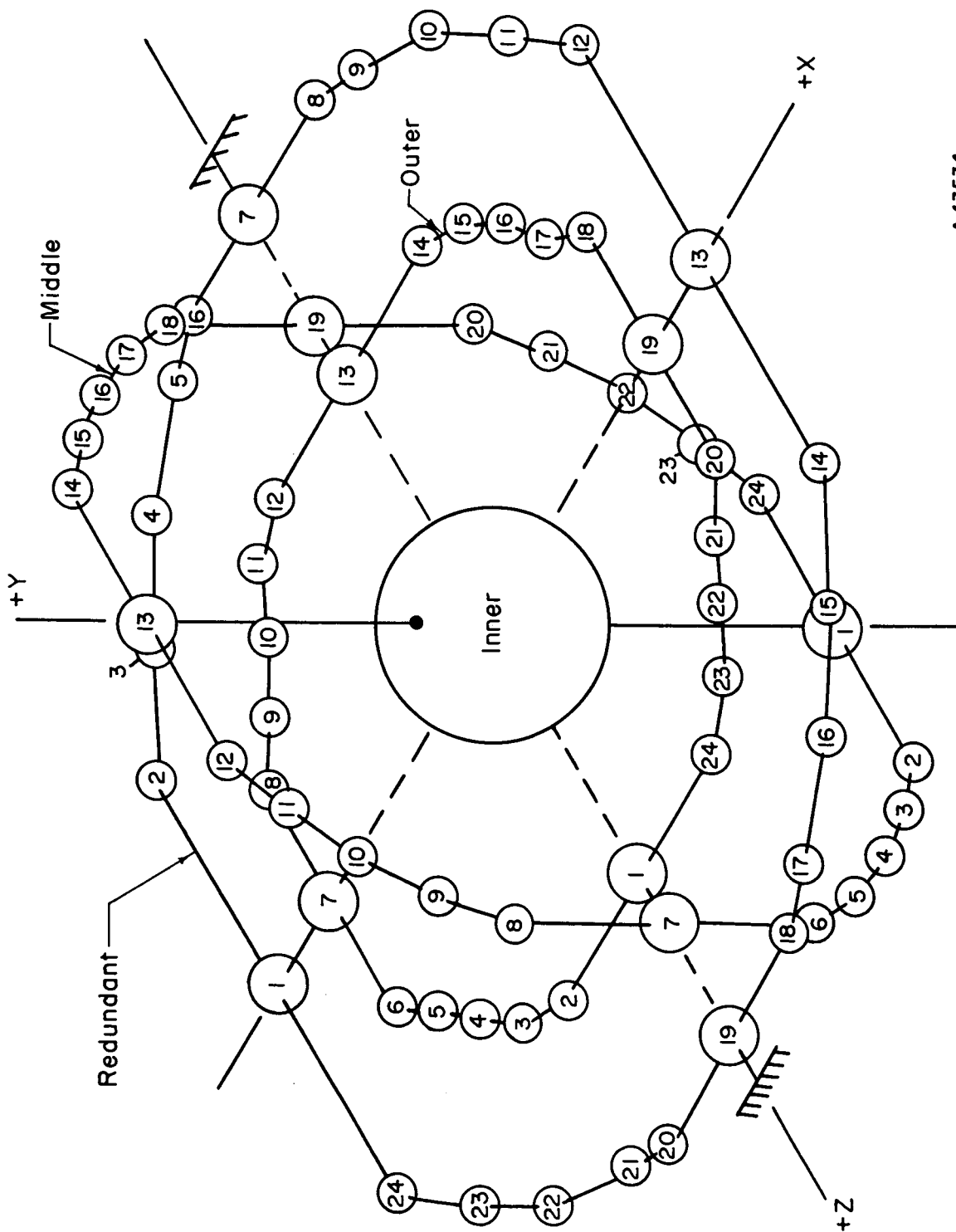
FIGURE D-1. MATHEMATICAL MODEL

A 43534

TABLE D-1. NODE COORDINATES AND MASSES[a]

Node	X, inches	Y, inches	Z, inches	Mass, 10^{-4} lb-sec^2 inches

A. Middle Gimbal

Node	X, inches	Y, inches	Z, inches	Mass
1	0	-6.25	0	98.00
2	0	-6.25	+2.75	4.16
3	0	-5.65	+3.86	1.63
4	0	-4.83	+4.83	1.48
5	0	-3.86	+5.65	1.63
6	0	-2.75	+6.25	4.16
7	0	0	+6.25	70.60

Symmetrical about Y and Z axis

B. Outer Gimbal

Node	X, inches	Y, inches	Z, inches	Mass
1	0	0	+5.19	46.50
2	-2.56	0	+5.19	3.19
3	-3.56	0	+4.68	1.96
4	-4.38	0	+3.92	1.96
5	-5.00	0	+3.00	2.03
6	-5.88	0	+2.25	3.33
7	-5.88	0	0	47.60

Symmetrical about X and Z axis

C. Redundant Gimbal

Node	X, inches	Y, inches	Z, inches	Mass
1	-7.63	0	0	81.40
2	-7.63	0	-4.25	8.32
3	-6.48	0	-5.86	5.46
4	-5.00	0	-7.17	5.46
5	-3.25	0	-8.13	4.28
6	-2.25	0	-8.63	4.51
7	0	0	-8.63	61.50

Symmetrical about X and Z axis

[a] Mass of inner gimbal = 662 x 10^{-4}.

TABLE D-2. GEOMETRICAL PROPERTIES OF MIDDLE
GIMBAL

Beam	L, inches	A, inches^2	I_x, inches^4	I_z, inches^4	$S^{(a)}$, 10^6 in-lb radians
A. Proposed Design					
1-2	2.75	1.780	5.000	0.2500	2.00
2-3	1.26	0.683	0.479	0.0282	0.70
3-4	1.27	0.683	0.479	0.0282	0.70
4-5	1.27	0.683	0.479	0.0282	0.70
5-6	1.26	0.683	0.479	0.0282	0.70
6-7	2.75	1.780	5.000	0.2500	2.00
B. Present Design					
1-2	2.75	2.32	15.00	0.290	4.80
2-3	1.26	2.32	5.10	0.100	6.70
3-4	1.27	2.32	5.10	0.100	6.70
4-5	1.27	2.32	5.10	0.100	6.70
5-6	1.26	2.32	5.10	0.100	6.70
6-7	2.75	2.32	15.00	0.290	4.80

(a) Torsional rigidity:

$$S = \frac{T}{\theta}$$

θ = total angle of twist of the beam

T = torque applied at ends of beam.

TABLE D-3. GEOMETRICAL PROPERTIES OF OUTER GIMBAL

Beam	$L,$ inches	$A,$ inches^2	$I_x,$ inches^4	$I_z,$ inches^4	$S,$ 10^6 in-lb / radians
A. Proposed Design				
1-2	2.56	2.000	5.000	0.2500	2.28
2-3	1.12	0.889	0.670	0.0336	1.35
3-4	1.12	0.889	0.670	0.0336	1.35
4-5	1.12	0.889	0.670	0.0336	1.35
5-6	1.16	2.000	1.000	0.0880	5.25
6-7	2.25	2.000	5.000	0.2500	2.60
B. Present Design				
1-2	2.56	2.32	15.00	0.2900	5.20
2-3	1.12	2.32	5.10	0.1000	7.60
3-4	1.12	2.32	5.10	0.1000	7.60
4-5	1.12	2.32	5.10	0.1000	7.60
5-6	1.16	2.32	5.10	0.1000	7.60
6-7	2.25	2.32	15.00	0.2900	5.90

TABLE D-4. GEOMETRICAL PROPERTIES OF REDUNDANT
GIMBAL

Beam	L, inches	A, inches^2	I_x, inches^4	I_z, inches^4	S, 10^6 in-lb radians
A. Proposed Design					
1-2	4.25	1.88	2.00	0.1000	2.00
2-3	1.98	1.44	1.16	0.0293	0.80
3-4	1.98	1.44	1.16	0.0293	0.80
4-5	1.98	1.44	1.16	0.0293	0.80
5-6	1.12	1.88	1.41	0.0610	1.10
6-7	2.25	1.88	5.00	0.2500	2.00
B. Present Design					
1-2	4.25	3.20	15.00	0.2500	4.80
2-3	1.98	3.20	12.40	0.1270	1.10
3-4	1.98	3.20	12.40	0.1270	1.10
4-5	1.98	3.20	12.40	0.1270	1.10
5-6	1.12	3.20	12.40	0.1270	2.00
6-7	2.25	3.20	20.00	0.5000	2.00